Alkaline Redox Flow Batteries

IISER PUNE

A Thesis submitted to

Indian Institute of Science Education and Research Pune in partial fulfilment of
the requirements for the BS-MS Dual Degree Programme

by

Mahendra Patel

EPFL

Supervisor

Prof. Hubert. H. Girault

Professor, Institute of Chemical Sciences and Engineering (ISIC)
École Polytechnique Fédérale de Lausanne, Valais Wallis,
Switzerland

List of Content

CERTIFICATE

This is to certify that this dissertation entitled **"Alkaline Redox Flow batteries"** towards the partial fulfilment of the BS-MS dual degree programme at the Indian Institute of Science Education and Research, Pune represents study/work carried out by **Mahendra Patel (Reg. No. 20151127)** at **École Polytechnique Fédérale de Lausanne, Sion, Switzerland under the supervision of Prof. Hubert H. Girault, Director LEPA (Laboratoire d'Electrochimie Physique et Analytique)** during the academic year 2019-2020.

Mahendra Patel
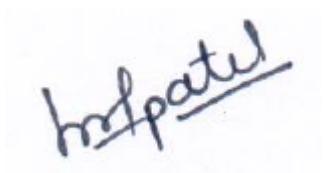
Prof. Hubert H. Girault

Director, LEPA

EPFL , Switzerland

Date: 19.03.2020

DECLARATION

I hereby declare that the matter embodied in the report entitled **"Alkaline Redox Flow Batteries"** are the results of the work carried out by me at the **École Polytechnique Fédérale de Lausanne, LEPA (Laboratoire d'Electrochimie Physique et Analytique)**, **Sion, Switzerland** under the supervision of **Prof. Hubert H. Girault** and the same has not been submitted elsewhere for any other degree.

Mahendra Patel

Prof. Hubert H. Girault

Director, LEPA

EPFL , Switzerland

Date: 19.03.2020

ACKNOWLEDGEMENTS

I would like to thank my supervisor, **Prof. Hubert Girault**, for giving me the opportunity to work in his group, and his valuable suggestions during the group meetings were very valuable and ensured constant progress of this project. Working under his guidance was a privilege not just because of his unbound endurance but also because of his incredibly helpful support.

I would also like to thank to my co-supervisor, **Dr. Solène Gentil,** who was constantly guide me. She has been a great leader and great support throughout my thesis work and invaluable suggestions every step of my thesis.

I would like to thank TAC member at IISER Pune, **Dr. Muhammed Musthafa O. T.,** for his constant support and suggestions.

I would like to thank you to Madame Patricia Byron for her support in administrative works. I would also like to thank Cedric Passerini for IT support and Stephane Voeffray for mechanical workshop at EPFL.

I would also like to thank especially to my housemate Seba Kader for his unconditional help and support during my time here.

Finally, I want to thank my parents, who always supported me selflessly and making me a person I am today.

Mahendra Patel

List of Figures

List of Tables

Abstract

Redox flow batteries (RFBs) are rapidly emerging as the one of the most practical solution for grid-scale energy storage and energy management due to their relative simplicity, high performance, long lifetimes and decoupled power and capacity. In addition, the use of redox active organic molecules to store energy have several advantages than other conventional redox flow battery (*e.g.*, vanadium-based) such as higher energy efficiency, solubility, multiple number of electron transfer and rapid electron transfer kinetics. In this work, we reported the organic electrolyte based alkaline redox flow battery using reactants composed of only earth-abundant material which are nonflammable, not expansive, non-toxic and working in alkaline medium (pH = 14). Alloxazine ester, inspired from vitamin B12 structure, was used at the negative side of the RFB and ferrocyanide or manganate were used at the positive side. The use of manganate at the positive side was investigated at concentration up to 100 mM and limited by manganese oxide platting on the battery components (electrodes and membrane). As a consequence, ferrocyanide was used as posolyte for battery cycling at higher concentration (0.4 M ferrocyanide at the positive side and 0.38 M alloxazine ester at the negative side). Finally, the alkaline RFB reached high performances up to 100 cycles with the volumetric capacity of 17.41 Ah L^{-1} including 98 % coulombic efficiency per cycle and average voltage and energy efficiencies of 91 % and 90%, respectively.

Chapter 1

Introduction

1.1 Energy storage technologies

At present, the supply of the power to industry and transports are mostly generated from non-renewable energy resources such as coal, fossil fuel and natural gas.[1] However, their effects on environmental pollution and the depletion of fossil resources expose the world to a serious global energy crisis.[1] The recent development of energy production based on renewable resources such as wind or solar, biomass, geothermal energies requires a reliable way to store theses energies.[2] The power output of renewable resources varies a lot during the day and night depending on the light intensity and wind speed, respectively. For example, energy production from solar panel depends on the weather conditions, which make their energy production very hard to predict. The intermittent energy production of renewable energy does not fit properly with the current energy demand. Therefore, there is a crucial need for large scale energy storage systems which can provide an alternative solution to the issues of the decoupling power generation and consumption.[3, 4]

Therefore, storing the excess of energy generated by the renewable sources into electrochemical energy storage systems (EESS) could be used to address, for example, the need of energy when the demand is high. Batteries are common EESS and are storing electrical energy by converting the chemical energy. For large scale grid applications, the most considered batteries have been sodium-sulfur batteries (Na-S), lithium-ion batteries (Li-ion) and redox flow batteries (RFBs).[4,5] Properties of each system are depicted in the Table1. The required properties to be used as storing technologies are high efficiency, high number of charge/discharge cycles and reasonable costs.[6] RFBs are type of battery that seems to fit these requirements.[7]

1.2 Comparison to Li-ion battery in terms of performances

The redox flow batteries have a low volumetric energy density (10-40 Wh L^{-1}) as compared to Li-ion (233 Wh L^{-1}).[4,8] Li-ion batteries are suitable for both mobile and stationary applications. The main limitation includes lithium dendrite formation with

high packaging cost and flammability of solid electrolytes used in such system. As a consequence, RFBs are considered as first choice owing to the cost of lithium as well as longer life time. Additionally, the safety concerns of the redox flow systems are very less, cyclability and stability are stupendous.[7]

Table 1: Technical characteristics for Li-ion, Na-S, and RFB [4,3,9].

Batteries	E density [Wh/kg]	Discharge time [h]	Cycle lifetime	T [°C]
Li-ion	100-200	1	600-1200	-10-40
Na-S	120-150	1	2500-4500	300-500
RFB	10-50	1-10	>10,000	10-50

1.3 Development of redox flow battery (RFBs)

The concept of redox flow battery developed from the National Aeronautics and Space Administration (NASA),[10] in the early seventies, derived from redox fuel cells, published by Posner and co-workers in 1955.[11] Redox flow batteries (RFBs) have many advantages over other energy storage systems as well as an excellent combination of energy efficiency, relatively low cost, long lifetime and low self-discharge.[12]

RFB stores energy by converting electrical energy into chemical energy through the oxidation and reduction of dissolved electro-active species in liquid electrolytes. By reversing these chemical reactions electrical energy can be recovered upon discharge. The electro-active species and electrolyte are stored externally on two separate reservoir tanks and are continuously pumped to flow through the electrodes located in the battery (Figure 1).[8] The electrochemical cell consists of a negative and positive electrode and an ion exchange membrane (IEM). The latter separates both electrolyte chambers while allowing transport of the charge carrying ions (*e.g.,* H^+, Cl^-, K^+,..) to maintain electrical neutrality and electrolyte balance. Both the electrodes are connected through the external circuit to an electric load during discharging and power source during charging.[12]
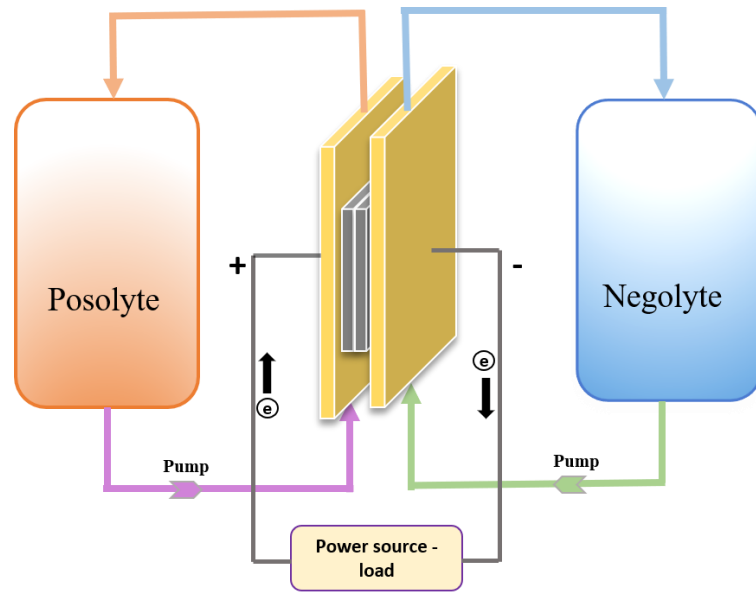
Figure 1: *Schematic of a redox flow battery.*

In order to charge the battery, a voltage is applied to the electrochemical cell. Oxidation reaction occurs on the positive side and reduction occurs on the negative side.[13]

$$\text{Positive side:} \quad A^x \rightarrow A^{x+n} + ne^- \tag{1}$$

$$\text{Negative side:} \quad B^y + ne^- \rightarrow B^{y-n} \tag{2}$$

During the discharging of the cell, current is opposite, and reverse reactions occurs (eq.3 and eq.4).[13]

$$\text{Positive side:} \quad A^{x+n} + ne^- \rightarrow A^x \tag{3}$$

$$\text{Negative side:} \quad B^{y-n} \rightarrow B^y + ne^- \tag{4}$$

As compared to other battery technologies (*e.g.*, Li-ion), power and energy are decoupled: the energy density depends on the redox species concentration and volume of electrolyte, while the power can be tuned by increasing the number the electrodes and their surface area.

1.4 RFB chemistries

During last few decades, a large variety of cathodic and anodic redox couples, suitable for RFBs, have been studied as mentioned in Table 2 and Table 3. The redox potential and solubility of the redox species are the main criterion that determines the battery's total energy density. The most investigated RFB's are all-vanadium and bromine-polysulfide. The technical characteristics of some RFB system are shown in Table 4.

Table 2: *A list of cathodic redox couples used in RFBs.*

Redox couples	E° [V *vs.* SHE]	Redox Reaction	References
V^{3+} / V^{2+}	-0.26	$V^{3+} + 1e^- \rightleftharpoons V^{2+}$	[14]
Cr^{3+} / Cr^{2+}	-0.41	$Cr^{3+} + 1e^- \rightleftharpoons Cr^{2+}$	[8]
S_4^{2-} / S_2^{2-}	-0.26	$S_4^{2-} + 2e^- \rightleftharpoons S_2^{2-}$	[8]
Fe^{2+} / Fe	-0.3	$Fe^{2+} + 2e^- \rightleftharpoons Fe$	[8]
Pb^{2+} / Pb	-0.13	$Pb^{2+} + 2e^- \rightleftharpoons Pb$	[8]
Zn^{2+} / Zn	-0.76	$Zn^{2+} + 2e^- \rightleftharpoons Zn$	[8]

Table 3: *A list of anodic redox couples used in RFB.*

Redox couples	E° [V *vs.* SHE]	Redox Reaction	References
VO_2^+ / VO^{2+}	+1.00	$VO_2^+ + 2H^+ + 1e^- \rightleftharpoons VO^{2+} + 2H_2O$	[15]
Fe^{3+} / Fe^{2+}	+0.77	$Fe^{3+} + 1e^- \rightleftharpoons Fe^{2+}$	[8]
Br_3^- / Br^-	+1.09	$Br_3^- + 2e^- \rightleftharpoons 3Br^-$	[8]
PbO_2 / Pb^{2+}	+1.49	$PbO_2 + 4H+ + 2e^- \rightleftharpoons Pb^{2+} + 2H_2O$	[8]
Ce^{4+} / Ce^{3+}	+1.75	$Ce^{4+} + 1e^- \rightleftharpoons Ce^{3+}$	[16]
Mn^{3+} / Mn^{2+}	+1.51	$Mn^{3+} + 1e^- \rightleftharpoons Mn^{2+}$	[14]

Table 4: *Technical characteristics of different liquid phase RFB batteries*[17]

Batteries	Standard cell voltage (V)	Efficiency (%)
All- vanadium	1.3	80-90
Iron-chromium	1.2	40-50
Vanadium-Bromide	1.1	80
Zinc-Cerium	2.6	80-90
Bromine-Polysulphide	1.5	60-65
Iron-Iron	1.1	50
All-lead	1.5	60-65

1.5 Vanadium redox flow Battery (VRFBs)

Vanadium redox flow batteries are one of the most developed flow battery, which was pioneered by Maria Skyllas-Kazacos and co-workers in 1985.[14] The V^{3+}/V^{2+} redox couple works in the negative half-cell, and the V^{5+}/V^{4+} redox couple works in the positive half cells as mentioned in Figure 2. These four stable oxidation states, dissolved in acidic aqueous solutions (1.6 M of vanadium ions in 2 M H_2SO_4), are characterized by their own colour: V^{2+} (violet), V^{3+} (green), V^{4+} (blue), V^{5+} (yellow). During the discharge, V^{2+} is oxidized to V^{3+} (eq.5) in the negative side (anode), while V^{5+} is reduced to V^{4+} (eq.6) at the positive side (cathode).[18] The two redox reactions are depicted below: [18]

Negative side: $V^{2+} \rightarrow V^{3+} + e^-$ $\qquad\qquad$ $E° = -0.26$ V *vs.* SHE $\qquad$ (5)

Positive side: $VO^+_2 + e^- + 2H^+ \rightarrow VO^{2+} + H_2O$ $E° = +1.00$V *vs.* SHE $\qquad$ (6)
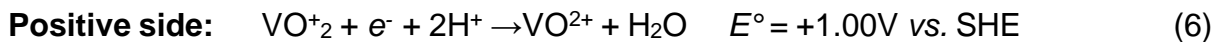
The use of the same element at various oxidation states minimizes crossovers through the membrane. An energy density around 40 Wh L^{-1} is achieved in this system at the maximum solubility limit of vanadium species.[19]
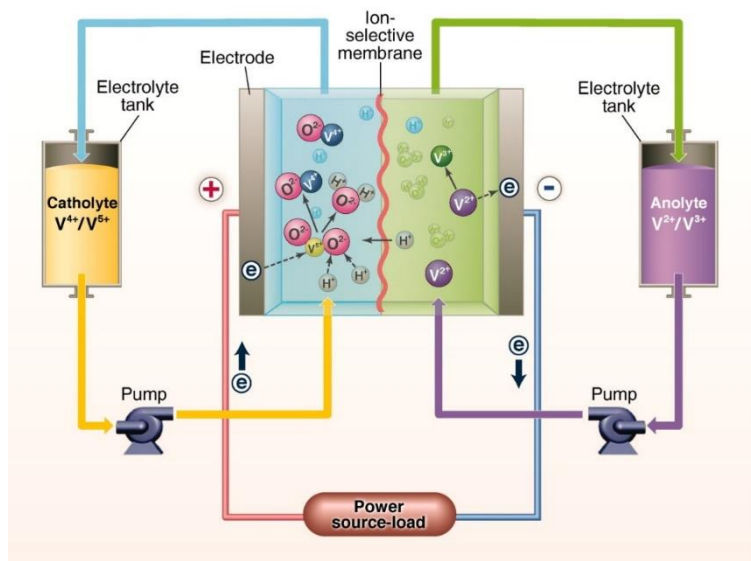
Figure 2: Schematic representation of a Vanadium Redox Flow Battery[4].

The main advantages of vanadium flow battery are high durability over more than 10000-20000 charge/discharge cycles and their stability against crossover of the vanadium species. Vanadium RFBs such as all-vanadium, iron/vanadium, cerium/vanadium, vanadium/air RFBs reached the phase of commercial development for large scale energy storage.[20] However, major drawbacks of these batteries are the low energy density. Indeed, the energy density of the battery is limited by the solubility of the vanadium species in the electrolyte, the range of the concentration is (1-2M) and the corresponding energy density is approximately 25-40 Wh L^{-1}. Furthermore, the fluctuating cost of vanadium pentoxide and the limited resources of vanadium metal on Earth drive the research to the development of more Earth-abundant electrolytes.[21]

Scientists have implemented water soluble redox active organic molecules into RFBs, which are low cost, easy to synthetize and non-flammable.[20] Therefore, aqueous organic redox flow battery (AO-RFB) are promising batteries for the clean-energy storage system.

1.6 Aqueous organic redox flow battery (AO-RFBs)

Implementation of water soluble redox active organic molecules opens a new opportunity for AO-RFBs to reduce the electrolyte cost and easily tune their properties. Chemical modifications by addition of various functional groups can improve the

17

solubility, the redox potential, the cell voltage, the energy density, and provide a multiple electron transfer with fast kinetics.[22, 23]

Aqueous organic redox flow batteries have several advantages over the other flow batteries:

- They have high thermodynamic standard potentials and high-specific charge storage capacity due to molecules with low molecular weight.
- Aqueous electrolytes have safety benefits since they do not contain any flammable electrolytes.
- Aqueous electrolytes are inexpensive since they consist of water and inorganic salts such as NaCl and KOH.[24,25]

The limitations of the aqueous redox flow batteries are the following:

- The water potential window is controlled by hydrogen and oxygen evolution reactions, so called HER and OER and the cell potential is limited to 1.23 V. The latter strongly depends on the pH and the potential window is larger in alkaline conditions (1.5-1.6 V)
- Chemical degradations of the redox species decrease the overall efficiency of the RFB.[26] Major chemical degradation mechanisms are nucleophilic addition, hydrolysis, self-oxidation and self-polymerization.

Over the last 5 years, several organic and organometallic RBFs have been reported in different environment such as acidic, alkaline or neutral conditions and are based on TEMPO, anthraquinone, quinone, methyl viologen and ferrocene derivatives.[23]

Wang *et al.* reported a low cost and sustainable AO-RFB using organic radical 4-hydroxy-TEMPO (catholyte) and methyl viologen (MV, anolyte) with NaCl as supporting electrolyte at neutral pH. The operating cell voltage of the battery is 1.25 V. Nevertheless, the effective capacity of the anolyte (3.0 M MV) was 43.2 Ah L^{-1}, and the overall performance of the battery is restricted by the catholyte solubility limit (4-hydroxy-TEMPO, < 0.5 M in NaCl). Finally, a volumetric energy density of 8.4 Wh L^{-1} was achieved. The battery operated at high current densities ranging from 20 to 100 mA cm^{-2} and achieved a coulombic efficiency of 100% over 100 cycles.[27]

Aziz *et al.* reported another metal free organic-inorganic aqueous redox flow battery using 9,10-anthraquinone-2,7-disulfonic acid (AQDS) at the positive side and bromine redox couples at the negative side with fast kinetic and reversible 2e^- transfer

process in sulfuric acid. A capacity retention of 99% per cycle and power density of 0.6 W cm^{-2} at 1.3 A cm^{-2} were demonstrated.[28]

1.7 Alkaline Redox flow batteries - State of the art

In order to increase the overpotential of the side reactions and the expected cell voltage, alkaline redox flow batteries were developed recently. Quinone and Alloxazine derivatives, inspired from vitamin B12 structure, were studied by Aziz group as promising candidates for alkaline redox flow batteries.[29] Aziz *et al.* reported the quinone based flow batteries in alkaline conditions (1 M KOH) using 2,6-dihydroxyanthraquinone (0.5 M) at the negative side and ferro/ferricyanide (0.4 M) at the positive side, with redox potential of -0.69 V *vs.* SHE and +0.51 V *vs.* SHE. The operating voltage of the battery is 1.2 V with the current and round-trip energy efficiencies of 99 and 84% with 0.1% capacity fading per cycle.[30]

Further, Aziz group reported another organic molecule as negative electrolyte using alloxazine 7/8-carboxylic acid in 1 M KOH. A one-step synthesis from o-phenylenediamine and alloxan gave a highly soluble redox molecule (2 M at pH 14) leading to a cell voltage of 1.2 V and capacity retention and energy efficiency of 99.98% and 63% over 400 cycles at a current density of 0.1 A cm^{-2}. Since alloxazine is not soluble in water, it has been altered to improve solubility by adding extra functional groups like COOH and OH.[29] Summary of organic based alkaline redox flow batteries are mentioned in Table.5.

Table 5: Summary of organic based alkaline redox flow batteries.

Negolyte	Posolyte	Cell potential	CE, EE	Ref.
0.5 M Alloxazine carboxylic acid (ACA)	0.4 M Ferrocyanide/40 mM ferricyanide	1.2 V	99.7 %, 74%	[29]
0.24 M Flavin mononucleotide	0.4 M Ferrocyanide	1.03 V	99%	[31]
0.5 M 2- hydroxy-3-carboxy-1,4-naphthoquinone (HCNQ)	0.4 M Ferrocyanide	1.02 V	94.7%	[32]

0.5 M 2,5-dihydroxy-1,4-benzoquinone (DHBQ)	0.4 M Ferrocyanide /ferricyanide	1.21 V	99.96 %, 37%	33
0.5 M 2,6-dihydroxyanthraquinone (DHAQ)	0.4 M ferrocyanide	1.2 V	99 %, 84%	30

1.8 Objectives of the Master Thesis

The objective of this thesis is to investigate novel redox couples for alkaline redox flow battery to increase the cell potential, electron transfer kinetic and efficiency of common RFBs. Therefore, we are introducing for the first time two electrolytes K_2MnO_4 and ferrocyanide for the positive side (posolyte) and alloxazine ester for the negative side (negolyte) using 1 M KOH as supporting electrolyte (pH 14). K_2MnO_4 was chosen because of its high electrochemical reversibility and high solubility in alkaline media.[34]

Figure 3 presents the flow cell in charging mode. Arrows indicate the direction of electron flow. The molecule structures of oxidized and reduced species are shown in the corresponding tank and redox reactions are mentioned below.
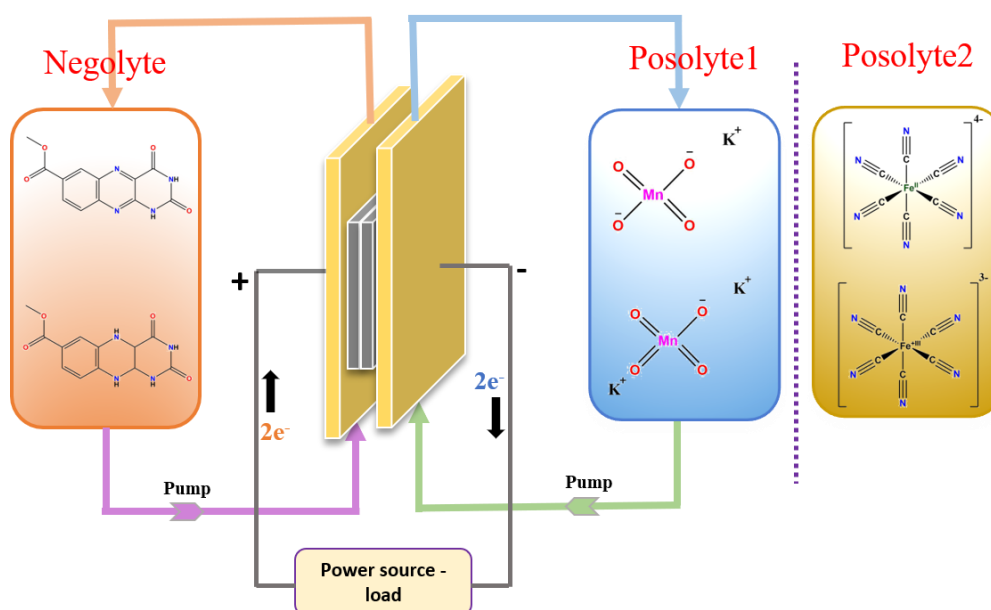
Figure 3: *Schematic scheme of alkaline redox flow battery in charging mode.*

Nagative side redox reaction:
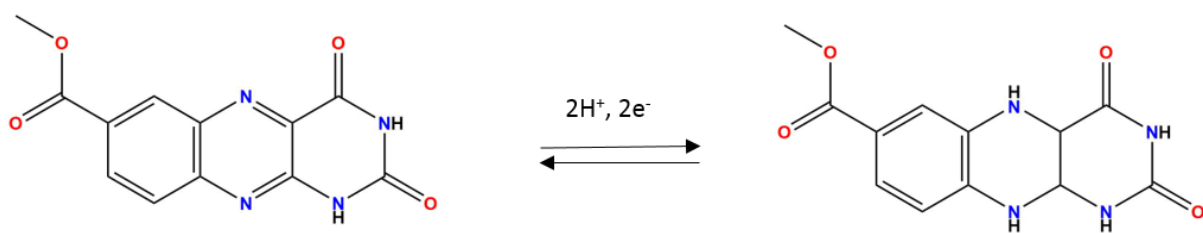
$$E° = -0.63 \text{ V } vs. \text{ SHE} \qquad (7)$$

Positive side redox reaction:

Posolyte 1 : $MnO_4^- + e^- \rightarrow MnO_4^{2-}$ $\qquad E° = +0.56 \text{ V } vs. \text{ SHE} \qquad (8)$

Posolyte 2 : $Fe(CN)_6^{3-} + e^- \rightarrow Fe(CN)_6^{4-}$ $\qquad E° = +0.51 \text{ V } vs. \text{ SHE} \qquad (9)$
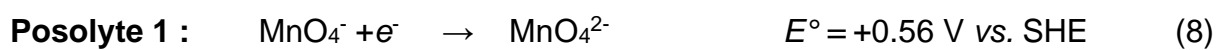
Chapter 2

Theoretical Part

2.1 Electrochemical cell: Three electrodes set-up

The three electrodes set-up is made of a working electrode (WE), a reference electrode (RE) and a counter electrode (CE). The working electrode is the electrode where the electrochemical reactions occurs. The reference electrode has a stable and well-defined electrode potential. The current is recorded in between the working electrode and counter electrode and the potential of the working electrode is measured according to the potential of the reference electrode. The three electrodes are connected to a potentiostat, which measures the electroanalytical phenomenon occurring in the electrochemical cell. Figure 4 illustrates an electrochemical cell with three electrode setups.
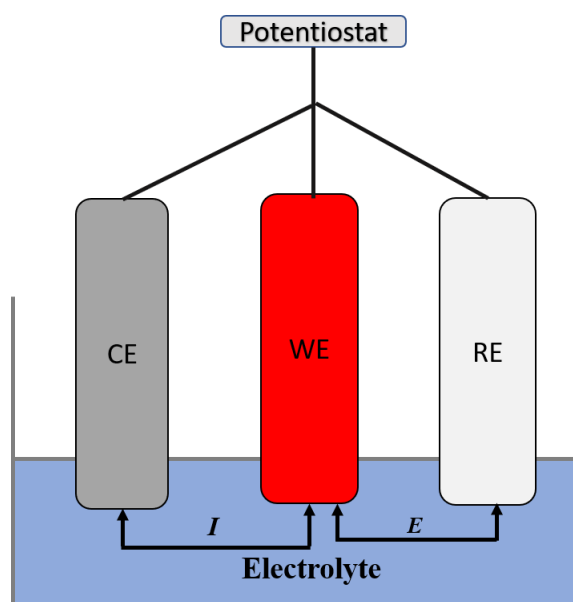
Figure 4: *Schematic representation of three- electrode setup in an electrochemical cell.*

2.2 Nernst equation

The Nernst equation relates the potential of redox species to the concentration of the oxidant and reductant.[35]

General electrochemical reduction reaction is mentioned below:

$$Ox + n\,e^- \rightarrow Red$$
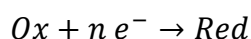
The Nernst equation is written as follow:

$$E = E° + RT/nF \cdot \ln\left(\frac{[Ox]^a}{[Red]^b}\right) \tag{10}$$

Where, E represents the potential of the redox species electrolyte (V) and $E°$ is the thermodynamic standard potential of the redox couple involved (V), R is the gas constant (J mol^{-1} K^{-1}), T the temperature (K), n the number of electrons exchanged, and F is the Faraday constant C mol^{-1}. [Ox] and [Red] are the concentration of oxidant and reductant respectively (mol L^{-1}) and finally a and b are the stoichiometric coefficients of the oxidant and reductant species in the redox equation.[36]

2.3 Beer-Lambert law

The Beer-Lambert law is the linear relationship between absorbance and concentration of absorbing species in the solution at particular wavelength (path length).

$$A = \epsilon \times l \times C \tag{11}$$

Where A is the absorbance of the sample at a given wavelength, ϵ is the molar extinction coefficient (L mol^{-1} cm^{-1}) of the species in the sample, C is the concentration of the analyte (mol L^{-1}) and l is the length of the sample (cm).

2.4 Cyclic voltammetry

Cyclic voltammetry (CV) is a useful potentiodynamic electrochemical measurement, in which the working electrode potential is ramped linearly versus time in a fixed potential window. The resulting current at the working electrode is then plotted versus the potential and the cyclic voltammogram is then obtained. An increase of the current in the positive values relates an oxidation process and an increase in the negative values shows a reduction. If the redox reaction is in equilibrium ($I_{p,ox}/I_{p,red} = 1$), the redox process is called reversible as shown in Figure 5.

The diffusion coefficient of the redox specie into the supporting electrolyte was estimated by CV by ranging the scan rate using the Randles-Sevcik equation:

$$Ip = (2.69 \times 10^5) n^{\frac{3}{2}} A D^{\frac{1}{2}} v^{\frac{1}{2}} C^*$$ (12)

Where, Ip = peak current (A), n = number of electron, A = geometrical area of the working electrode (cm^2), D = diffusion coefficient (cm^2 s^{-1}), C^*= concentration of the redox specie (mol cm^{-3}) and v = scan rate (V s^{-1}).
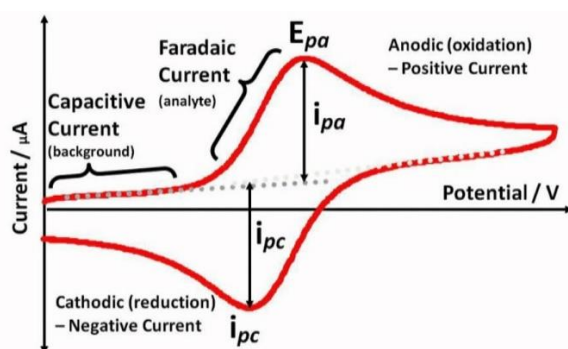
Figure 5: *Schematic representation of cyclic voltammogram for a reversible system[37].*

2.5 Rotating-Disk-Electrode (RDE)

The rotating-disk electrode, was used as hydrodynamic working electrode, to limit the diffusion layer thickness formed in the electrolyte upon mass-transport limitations (in stationary measurement).[38] In this technique, the electrode is uniformly accessible and the diffusion and convection of the reactant at the electrode surface is under control. The following equation describes the approximate diffusion layer thickness δ_o: where ω is the rotation rate in rpm.

$$\delta_o = 4.98 D^{\frac{1}{3}} v^{\frac{1}{6}} \omega^{\frac{-1}{2}}$$ (13)

The limiting current observed with RDE is reported by the Levich equation:

$$i_l = (0.62) n F A D^{\frac{2}{3}} v^{\frac{1}{6}} \omega^{\frac{1}{2}} C^*$$ (14)

Where, i_l = limiting current (A), n = number of electrons, ω = angular frequency (rad s^{-1}), v = kinematic viscosity (cm^2 s^{-1}), F = Faraday constant (C mol^{-1}), D = Diffusion coefficient (cm^2 s^{-1}), C^* = Analyte concentration (mol cm^{-3}).

If the redox process is reversible (with no involved chemical processes), the shape of wave should not depend on the ω. Therefore, the limiting current should be proportional to $\omega^{1/2}$ at any potential. On other hand if the shape of the curves depends on ω, then the redox process is kinetically limited. For the redox reaction, kinetic parameter such as rate constant and transfer coefficient can be estimated by using the Koutecky-Levich equation:[38]

$$\frac{1}{j} = \frac{1}{j_k} + \frac{1}{(0.62)n\,F\,A\,D^{\frac{2}{3}}\,v^{\frac{-1}{6}}\,\omega^{\frac{1}{2}}\,C} \tag{15}$$

Where, j is the total current density and j_k is the kinetic current density.
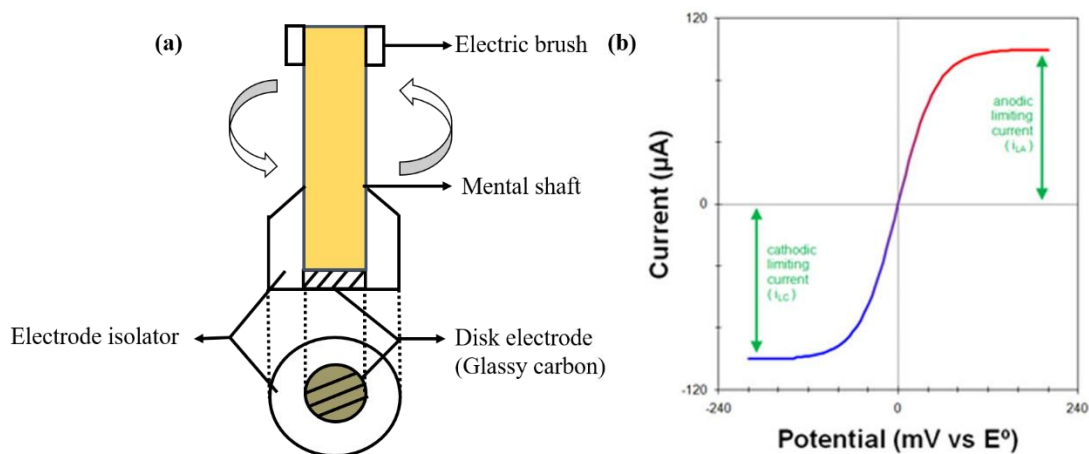
Figure 6: (a) Scheme of a rotating disk electrode (b) RDE voltammogram for both anodic and cathodic redox couples[39].

2.6 Battery efficiency

The efficiency of the battery is usually defined by the energy efficiency, which is the ratio of the electrical work recovered from the battery during discharging compared to the electrical work used for charging it.[36]

$$\eta_{Energy} = \frac{\int V_{discharge} \, dQ_{discharge}}{\int V_{charge} dQ_{charge}} = \frac{W_{discharge}}{W_{charge}} \qquad (16)$$

The energy efficiency can be decomposed in between the voltage and coulombic efficiencies.

$$\eta_{Energy} = \eta_{coulombic} \cdot \eta_{volatge} \qquad (17)$$

The coulombic efficiency considers the charge loss and is defined as the ratio between the charge output (discharging) and the charge input (charging). The charge losses are caused by either crossover of the electrochemical species through the membrane or side reactions.

$$\eta_{Coulombic} = \frac{\int I_{discharge} \, dt_{discharge}}{\int I_{charge} dI_{charge}} = \frac{Q_{discharge}}{Q_{charge}} \qquad (18)$$

The voltage efficiency is related to the voltage loss and is defined as the ratio between the average charging voltage compared to the average discharging voltage.

$$\eta_{Volatge} = \frac{Q_{discharge}}{Q_{charge}} = \frac{\frac{1}{t_{Discharge}} \int_0^{t_{Discharge}} V_{discharge} dt}{\frac{1}{t_{charge}} \int_0^{t_{Charge}} V_{Charge} dt} \qquad (19)$$

This efficiency is related to the overpotential of the system that is given by:

$$\eta = E_{measured} - E_{eq} = \eta_{kinetic} \eta_{mass-tranfer} + I \, R \qquad (20)$$

The overpotential is the difference between the potential at equilibrium (given by Nernst eq.7) and the potential measured under the current, and the ohmic drop (IR) of the system, where R is the resistance of the system (Ω) and I is the current driven in the system (A).[36]

Chapter 3

Experimental Methods

3.1 Chemicals

Alloxan monohydrate ($C_4H_2N_2O_4 \cdot H_2O$, 98%) and acetic acid ($C_2H_4O_2$, 99.5%) were purchased from Acros Organics, and methyl 3,4-diaminobenzoate ($C_8H_{10}N_2O_2$, 98%) was purchased from Alfa Aesar. Boric Acid (H_3BO_3, 99.5%) and diethyl ether (($C_2H_5)_2O$, 99%) were purchased from Sigma Aldrich. Electrolyte solution was prepared from Potassium hexacyanoferrate(III) ($K_3Fe(CN)_6$, 99% Fulka), Potassium hexacyanoferrate(II) trihydrate ($K_4Fe(CN)_6.3H_2O$, 99% Acros), Potassium permanganate ($KMnO_4$, 97% Fulka) and Potassium hydroxide (KOH, 85% pellets, Sigma Aldrich).

3.2 Synthesis of alloxazine ester

Alloxan monohydrate (3.12 mmol, n_{eq} = 1, MW= 160.09 g mol^{-1}) and boric acid (3.12 mmol, n_{eq}= 1, MW=61.83 g mol^{-1}) was added into 60 mL of acetic acid. The reaction mixture was stirred at 70°C at atmospheric pressure under nitrogen. Methyl 3,4-diaminobenzoate (3.12 mmol, n_{eq}=1, MW= 166.18) was added in 30 mL of acetic acid and the solution was bubbled with N_2 for 30 min. Methyl 3,4-diaminobenzoate solution was then added quickly (avoid the precipitation) in the alloxan/boric acid solution. After the reaction (4 days), the product was collected by vacuum filtration, washed with acetic acid, water, and diethyl ether, and dried rotary evaporator. The yield was obtained 94%.
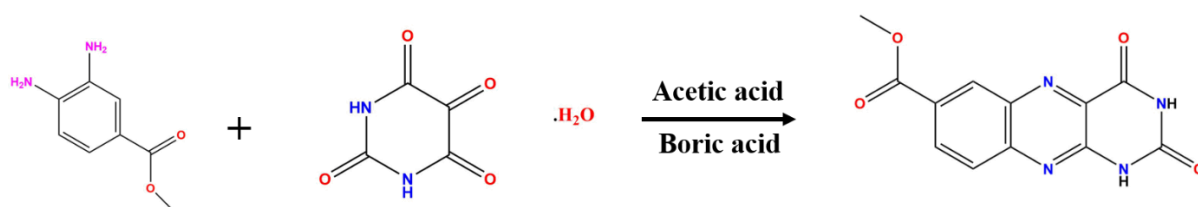
Figure 7: *Synthetic scheme of alloxazine ester.*

To characterize the final product, ^{1}H NMR spectra were recorded using routine NMR spectrometers operating at 400MHz. Major isomer:^{1}H NMR (400 MHz, DMSO) δ 12.10 (s, 2H), 11.84 (s, 2H), 8.66 (d, J = 1.9 Hz, 1H), 8.40 (d, J = 1.8 Hz, 1H), 8.34 (dd, J = 8.8, 2.0 Hz, 1H), 8.28 (d, J = 8.8 Hz, 1H), 8.18 (dd, J = 8.7, 1.9 Hz, 1H), 8.00 (d, J = 8.8 Hz, 1H), 3.96 (d, J = 2.3 6H).
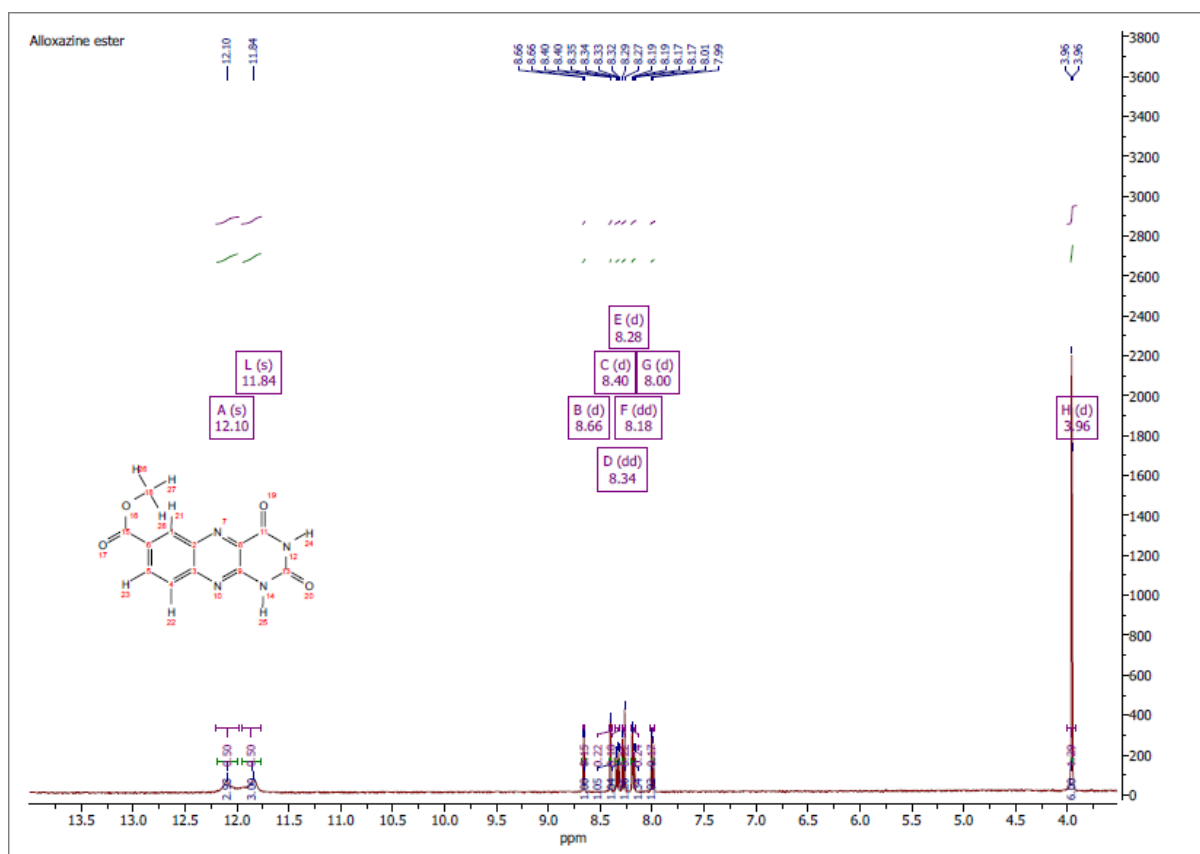
Figure 8: *^{1}H NMR (400 MHz, DMSO) spectrum of alloxazine ester.*

3.3 Electrochemical analysis

Electrochemical characterizations were done using the cyclic voltammetry (CV) and rotating disk electrode (RDE) experiments.

3.3.1 Cyclic voltammetry experiments

Cyclic voltammetry experiments were performed in alkaline medium 1 M KOH using an Autolab PGSTAT302N potentiostat-galvanostat. All the measurements were recorded at room temperature using NOVA software by Metrohm. CV were performed with a three-electrode setup using glassy carbon (0.071 cm^2) as a working electrode, platinum wire as a counter electrode, and homemade Ag/AgCl (3M KCl) as a reference electrode (low concentration of electrolytes like1 mM) and mercury reference electrode (higher concentration of electrolytes like 10 mM), regularly measured against a master Ag/AgCl (KCl sat) electrode (0.230V ±10mV). The electrodes were polished using alumina paste (1µM) before starting the experiments. Nitrogen gas was bubbled in the solution 10min before the beginning of the measurements to remove the O_2 from the solution. CV was recorded in different electrolytes like alloxazine ester, ferricyanide, ferrocyanide, $KMnO_4$ and K_2MnO_4 in 1M KOH using different scan rates.

3.3.2 Rotating-Disk electrode experiments

Rotating disk electrode experiments were performed using a Metrohm rotator instrument using similar setup as the one used in cyclic voltammetry. Linear sweep voltammetry (LSV) were performed on a 5mm diameter platinum disc in alloxazine ester, ferricyanide, ferrocyanide, $KMnO_4$ and K_2MnO_4 in 1M KOH. The electrodes were polished using alumina paste (1µM) before starting the experiments. Nitrogen gas was bubbled in the solution 10min before the beginning of the measurements. Counter electrode was the same used as similar to CV experiments and mercury oxide (Hg/HgO) electrode was used as reference electrode. The following rotation speed were used in the LSV experiments: 100, 200, 300, 400, 500, 600, 700, 800, 900,1000 rpm. The diffusion coefficient of the redox specie was calculated from the Levich equation.

3.4 Optical measurements

Absorption spectra were measured on a PerkinElmer UV−vis spectrophotometer Lambda 950s to know the solubility limit of alloxazine ester, ferricyanide, ferrocyanide, $KMnO_4$ and K_2MnO_4 in 1M KOH. A saturated solution of alloxazine ester was prepared by addition of the analyte until a precipitation formed. Additional 1M KOH was added to mix the suspension. The solution was mixed and stirred for 2 hours to make sure that no particles will be dissolved in the solution. Then, the suspension was centrifugated to collect the supernatant. The supernatant was diluted in 1M KOH solution and its absorbance was measured using the UV-vis spectrophotometer. In order to determine, the extinction molar coefficient of the redox specie in 1 M KOH, UV-vis spectroscopy was measured for at different concentrations (10, 20, 40, 60, 80, 100 μM). The obtained standard calibration curve (A vs C) was used to extract the extinction molar coefficient using the Beer-lambert law.

3.5 Surface Characterization

The morphological characterization of the electrode (carbon felt) before and after cell cycling were studied by scanning electron microscopy (SEM). SEM images were performed with a Teneo SEM (FEI, USA) equipped with a Schottky field emission gun using voltage range between 1 to 10kV and different magnification.

3.6 Flow cell experiments

The cell consists of two titanium current collector (positive and negative half-cells, respectively) connected to the external electrical circuit. Nafion® N117 ion exchange membrane (fuel cell store, USA) were used as a separator. The end plates were made of the polypropylene material because this material resists to alkaline medium. The electrodes were carbon felt (AvCarb Felt G200, fuel cell store, USA) with a geometrical area 2 cm^2 and a thickness 1mm. They were pre-treated by heating in an oven at 300°C overnight. Silicon and teflon gaskets were added in between the current collectors and membrane to improve the tightness and avoid cell leakages. The volume of the electrolytes was 10 mL in the negative side and 20 mL in the positive side. The electrolyte solutions were mechanically pumped (Masterfles L/S, Cole-Parmer) with the flow rate of 21ml min^{-1} (12rpm) through the electrochemical cell. Anaerobic conditions were achieved by flushing N_2 within the electrolyte reservoir,

continuously. The flow cell performances were recorded by galvanostatically controlled potential-limited techniques at various current using EC-Lab software. The flow cell measurement was performed in a three-electrode setup configuration using mercury/mercury oxide as a reference electrode. A picture of the flow cell setup is depicted in Figure 9.
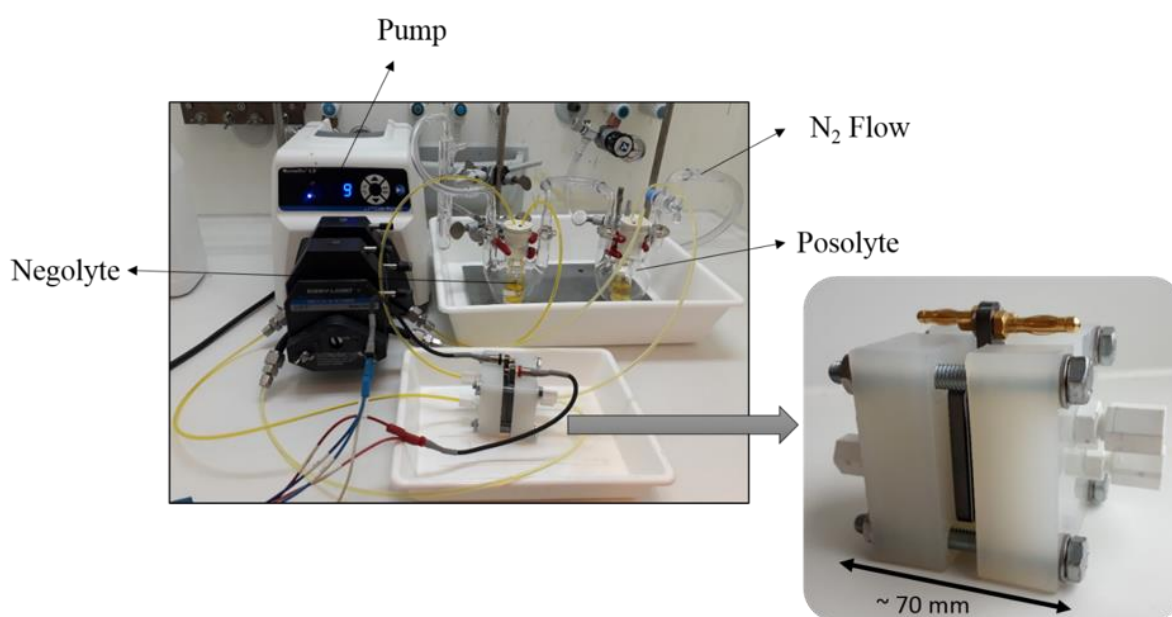
Figure 9: Flow cell setup during cell cycling.

When the concentration of electrolytes was increased up to 100 mM, the viscosity of the electrolyte was significantly higher, leading to mass transport limitations. As a consequence, the battery setup was slightly changed: the electrode surface area was increased to 8cm^2 and the electrode thickness was fixed to 6mm. The flow rate was enhanced to 25ml min^{-1} (14 rpm). In higher concentration , we were use the 5mm gold coated titanium current collector as shown in Figure 9 to avoid the corrosion in current collector during the flow of the electrolytes. The picture of the big flow cell is depicted in Figure 10.
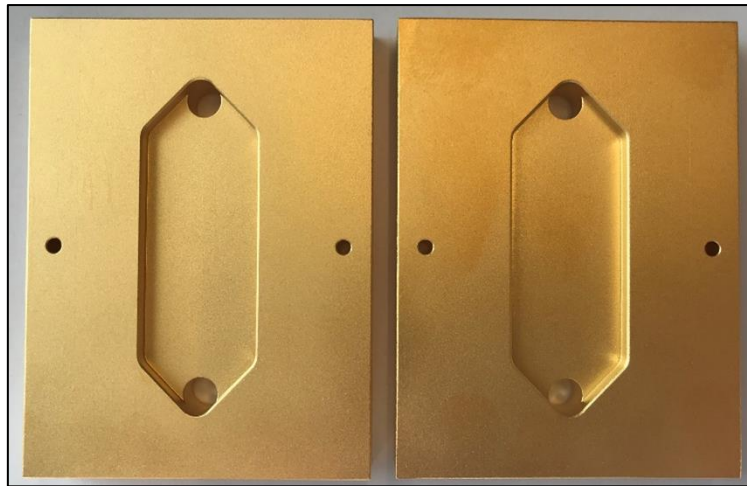
Figure 10: Picture of gold-coated titanium current collector.
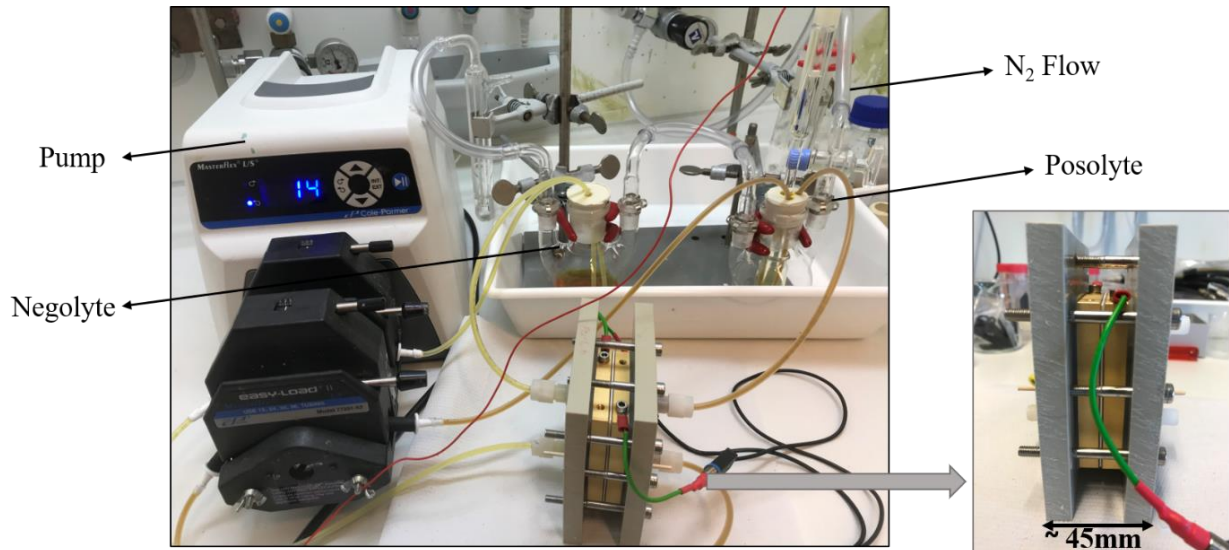
Figure 11: Big flow-cell setup used during cell cycling.

Chapter 4

Results and Discussion

In order to know the solubility limit of the redox species, redox properties of the electrolyte, Ultraviolet-visible spectroscopy, cyclic voltammetry (CV), rotating disk electrode (RDE) were first performed.

4.1 UV-Vis and solubility measurements

UV-Vis measurements were performed in order to determine the solubility limit of the redox species used as posolyte and negolyte at various pH conditions (1 M KOH, pH 14 and 0.5 M sodium carbonate buffer, fixed at pH 10). The absorption spectrum at various concentrations obtained for alloxazine ester at pH 10 and 14 are mentioned on Table 6.
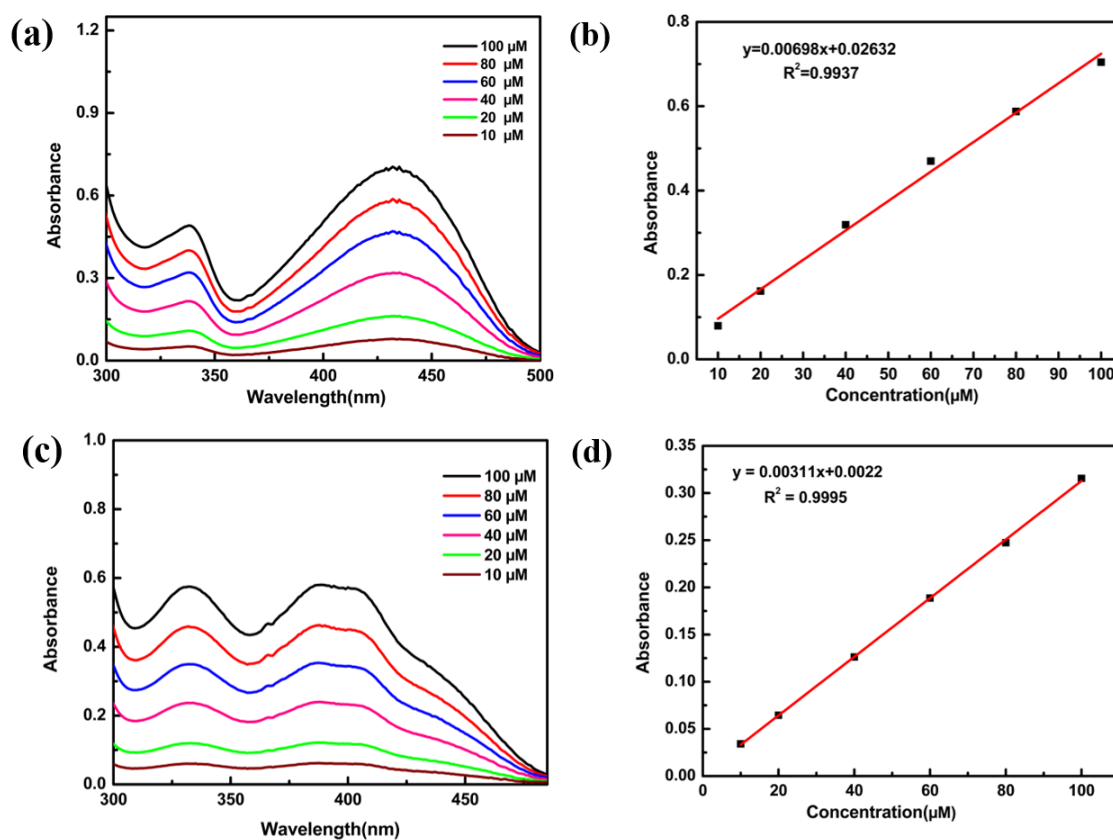
Figure 12: *(a) UV-vis spectra of alloxazine ester in 1M KOH at different concentrations. (b) Standard calibration curve of alloxazine ester at the maximum*

absorption peak of 434 nm. (c) UV-vis spectra of alloxazine ester in pH 10 carbonate buffer at different concentrations (d) Standard calibration curve of alloxazine ester absorbance at the maximum absorption peak of 440 nm.

In 1 M KOH, the absorption peaks observed at 338 and 435 nm (Figure 12a) can be assigned to $\pi \rightarrow \pi^*$ transitions.[31] Whereas in pH 10 carbonate buffer, absorption peak were observed at 330 and 440 nm and can be also assigned to $\pi \rightarrow \pi^*$ transitions (Figure 12c).

The same experiments were performed for manganate and permanganate solution in 1 M KOH (Figure 13). For $KMnO_4$, the absorption peaks were observed at 545, 525, and 348 nm (Figure 13c), attributed to ligand to metal charge transfer (LMCT) transitons.[40] In the case of K_2MnO_4, absorption peaks were found at 603, 437 and 351 nm (Figure 13a), and transition types are the same as $KMnO_4$.
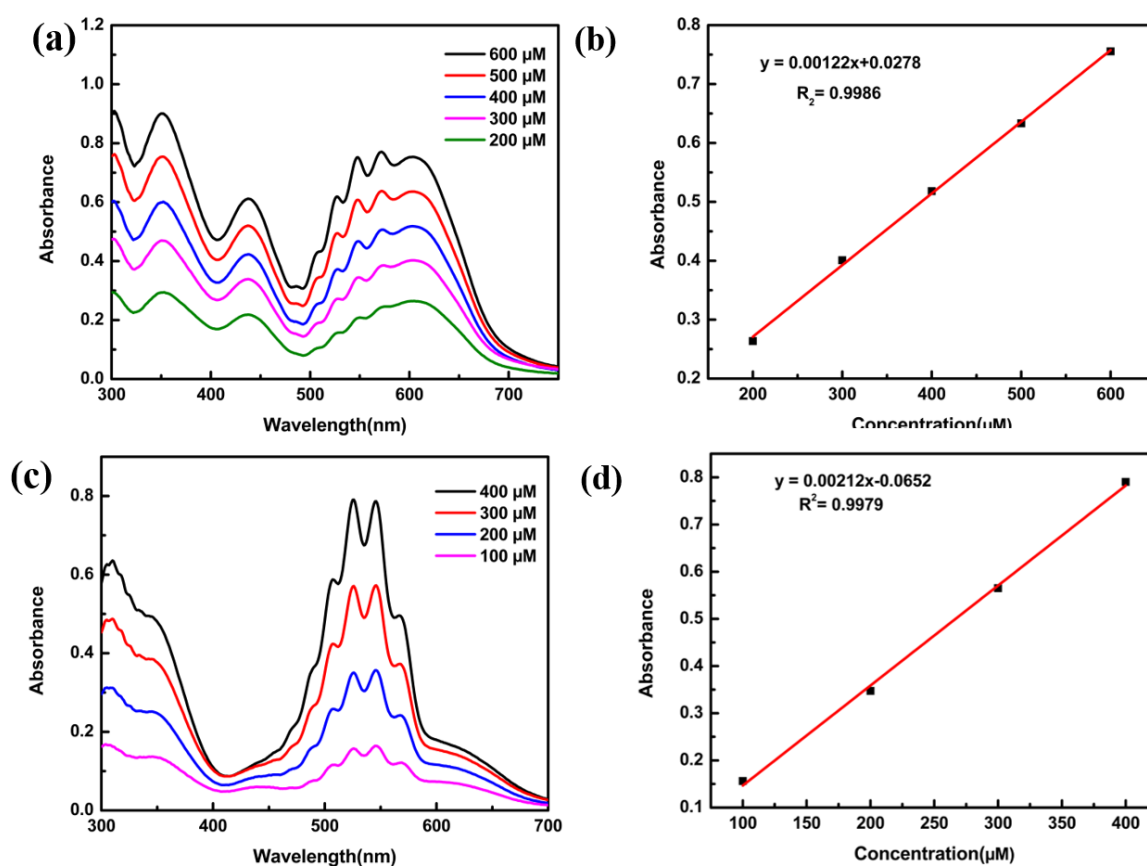
Figure 13: (a) UV-vis spectra of K_2MnO_4 in 1M KOH at different concentrations, (b) Standard calibration curve of K_2MnO_4 absorbance at 603 nm, (c) UV-vis spectra of $KMnO_4$ at different concentrations,(d) Standard calibration curve of alloxazine ester absorbance at 545 nm.

Another important parameter is the solubility of the active species dissolved in the supporting electrolyte, since it correlates to the energy density of the redox flow battery. In the case of alloxazine ester, the solubility limit is higher in KOH medium (0.38 M) than 0.5 M sodium carbonate buffer (0.62mM) pH10, as mentioned in Table. 6. We believe that the carbonate buffer (CO_3^- ion) does not create a suitable solvation shell to dissolve the alloxazine ester, properly.[40] K_2MnO_4 and $KMnO_4$ are relatively soluble in 1 M KOH, reaching solubility limits of 0.38 and 0.24 M, respectively.

Table 6: Solubility limit of posolyte and negolyte.

Electrolytes	Solubility limit	Standard deviations	Molar Coefficient extinction ($M^{-1}cm^{-1}$)
Alloxazine ester in 1M KOH	0.38 M	0.075498	6479 at 434nm
Alloxazine ester in pH 10 buffer	0.63 mM	0.016113	3107 at 440nm
$KMnO_4$ in 1M KOH	0.25 M	0.03395	2121 at 545nm
K_2MnO_4 in 1M KOH	0.38 M	0.020664	1355 at 603nm
Ferrocyanide in 1M KOH	0.40 M [30]	-	-

4.2 Electrochemical analysis: Cyclic Voltammetry Studies (CV)

4.2.1 Alloxazine ester redox reaction

Cyclic voltammetry of 1 mM alloxazine ester in 1 M KOH at different scan rate is presented on Figure 13. The oxidation and reduction peaks are attributed to a two-electron and two proton transfer (Proton coupled electron transfer (PCET)) mechanism as shown on the mechanism (eq.7). Oxidation and reduction peaks were observed at -0.5 V and -0.8 V *vs.* SHE at 5mV s^{-1}, respectively. The standard potential of alloxazine ester is -0.63 V *vs.* SHE. The peak potential difference was around 300 mV at 5mV s^{-1} as shown in Figure 14c, and the maximum anodic and cathodic peak current densities were respectively 0.023 and -0.07 mA cm^{-2}. The larger separation between oxidation and reduction peaks can be explained by slow electron transfer kinetic. From

the Randles-Sevcik analysis (eq.9), the diffusion coefficient was measured to be $5.76*10^{-7}$ cm^2 s^{-1} as shown in Figure 14b, which is one order of magnitude lower than the diffusion coefficient of alloxazine carboxylic acid (ACA) found to be $5.9*10^{-6}cm^2$ s^{-1}.[41] From the Figure 14b, the peak current *vs.* square root of scan rate showing the straight line and it's not passing through the 0 it means we have probably an effect of absorption of the redox species at the electrode surface. However, the diffusion coefficient is not reliable from the Levich equation so further investigations were done using rotating-disk electrode (RDE) experiments to calculate the diffusion coefficient because in RDE the steady state current is limited by the flow of the solution.

Figure 14: *(a) Cyclic voltammogram of 1mM alloxazine ester in 1M KOH at different scan rate, (b) Plot of peak current vs. square root of scan rate, (c) Plot of anodic and cathodic peak potential vs. scan rate.*

In order to increase concentration of redox species in solution and study any possible influence onto electron transfer kinetic, electrochemical characterizations were performed at 10mM (Figure 15). The standard potential was found to be -0.63 V *vs.* SHE, in agreement with what was described by Aziz group for ACA (-0.62 V *vs.* SHE). [29] The peak potential difference of 10 mM alloxazine ester in 1 M KOH was 160 mV at

5mV s^{-1}, which is less than the 1mM alloxazine ester in 1M KOH as shown in Figure 15c, and the maximum anodic and cathodic peak current densities were respectively 0.31 and -0.81 mA cm^{-2}.When we increased the concentration of alloxazine ester (1mM to 10mM), we obsessed the pre-peak absorption at -0.9V *vs.* SHE. The diffusion coefficient at 10 mM was equaled to D = 2.79*10^{-7} cm^2 s^{-1} as shown in Figure 15b.
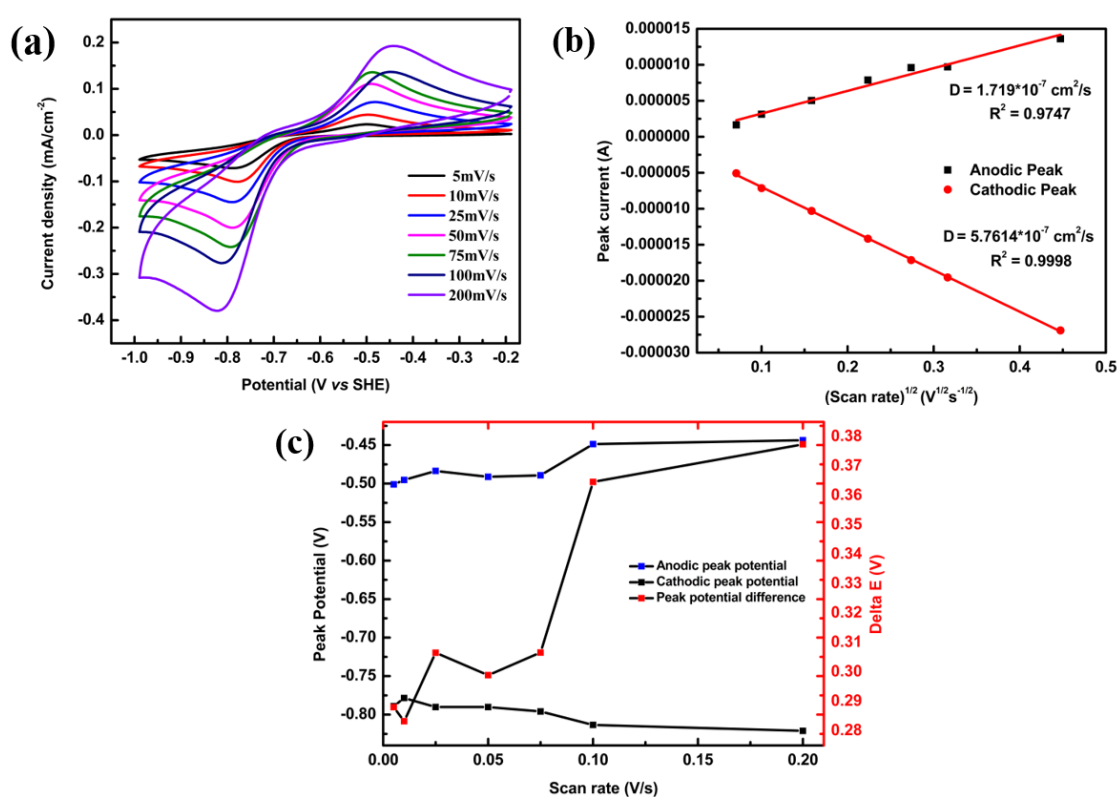

Figure 15: *(a) Cyclic voltammogram of 10mM alloxazine ester in 1M KOH at different scan rates, (b) Plot of peak current vs. square root of scan rate, (c) Plot of anodic and cathodic peak potential vs. scan rate.*

4.2.2 KMnO$_4$ redox reaction

Cyclic voltammetry of KMnO$_4$ (10mM) in 1 M KOH is shown in Figure 16. The oxidation and reduction peaks are attributed to a one electron transfer mechanism as shown on the redox mechanism in eq.8. As shown on Figure 16a, oxidation and reduction peaks were observed at 0.64 and 0.55 V *vs.* SHE at 5mV s^{-1}, respectively. The standard potential is about 0.558 V vs. SHE, as reported in the literature.[34] The peak potential difference between the oxidation and the reduction peaks was only 80 mV at 5 mV s^{-1} as shown in Figure 16c. Maximum anodic and cathodic peak current densities were respectively 0.38 and -0.65 mA cm^{-2}. From the Randles-Sevcik analysis, the diffusion

coefficient was measured to be $3.35*10^{-5}$ cm^2 s^{-1}, (Figure 16b) as similar to the reported values in literature.[42]

Figure 16: *(a) Cyclic voltammogram of 10mM KMnO₄ in 1M KOH at different scan rate, (b) Plot of peak current vs. square root of scan rate, (c) Plot of anodic and cathodic peak potential vs. scan rate.*

4.2.3 Ferricyanide redox reaction

Cyclic voltammetry of ferricyanide (10 mM) in 1M KOH was performed as shown on (Figure 17). The oxidation and reduction peaks are attributed to a one electron transfer mechanism as shown in eq.9. From Figure 17a, the oxidation peak was observed at 0.56V and reduction peak was observed at 0.4 V *vs.* SHE at 5mV s^{-1}. The standard potential is 0.47 V *vs.* SHE. The peak potential difference is about 140 mV at 5mV s^{-1} as shown in Figure.17c and the maximum anodic and cathodic peak current densities were respectively 0.22 and -0.46 mA cm^{-2} at 5mV/s. From the Randles-Sevcik analysis, the diffusion coefficient was measured to be $7.84*10^{-6}$ cm^2 s^{-1}, (Figure 17b) as reported in literature.[41] However, we were observed that as compared to

manganate, the ferricyanide showed a lower diffusion constant and an higher peak potential difference as well as slightly lower redox potential .
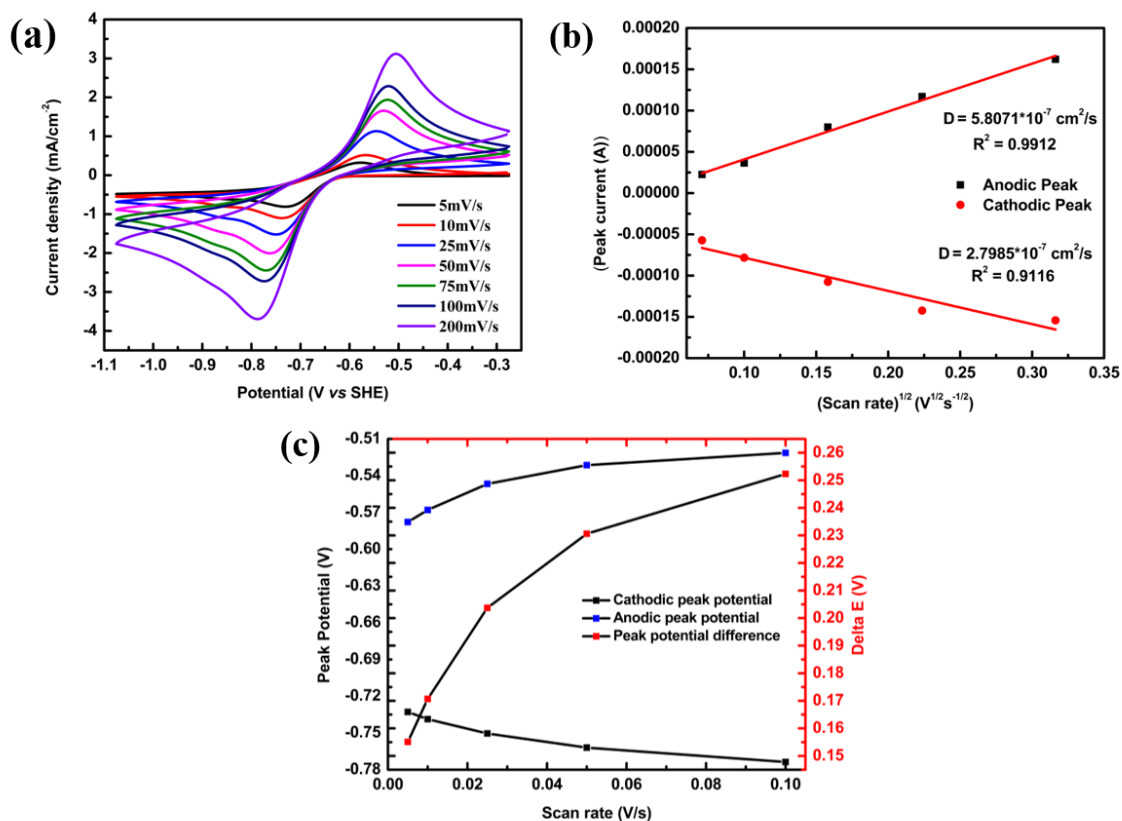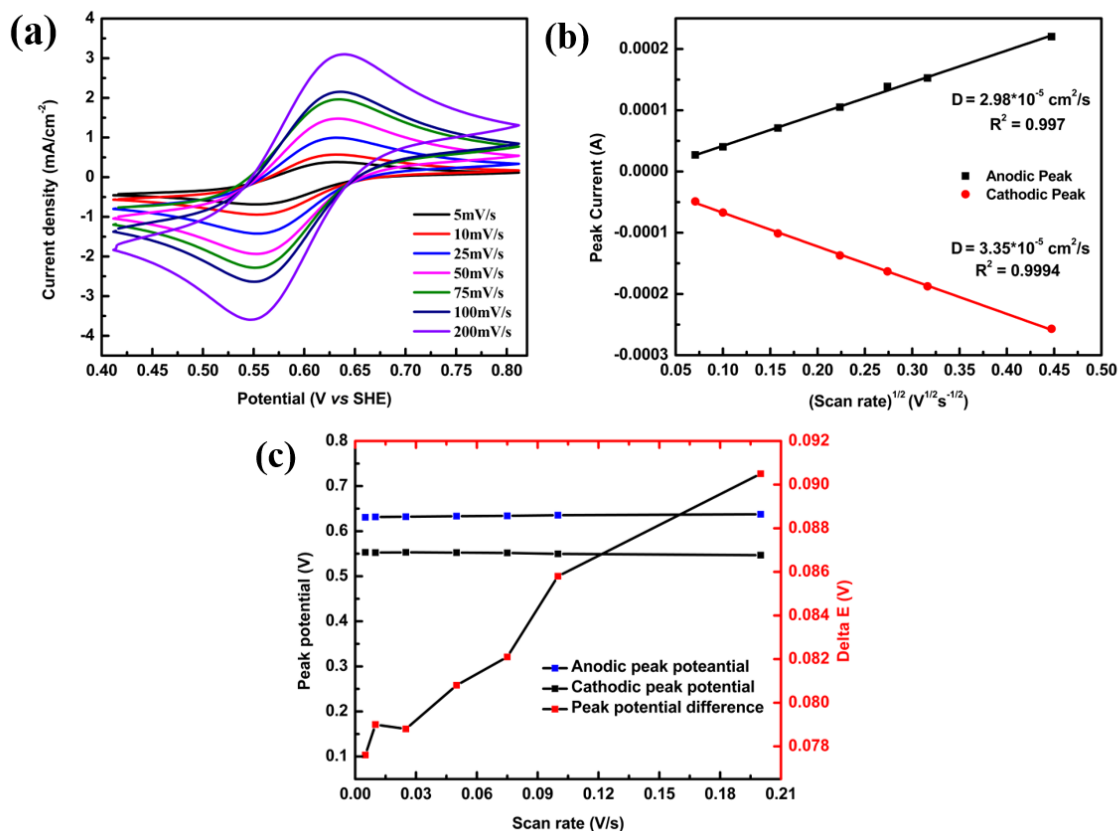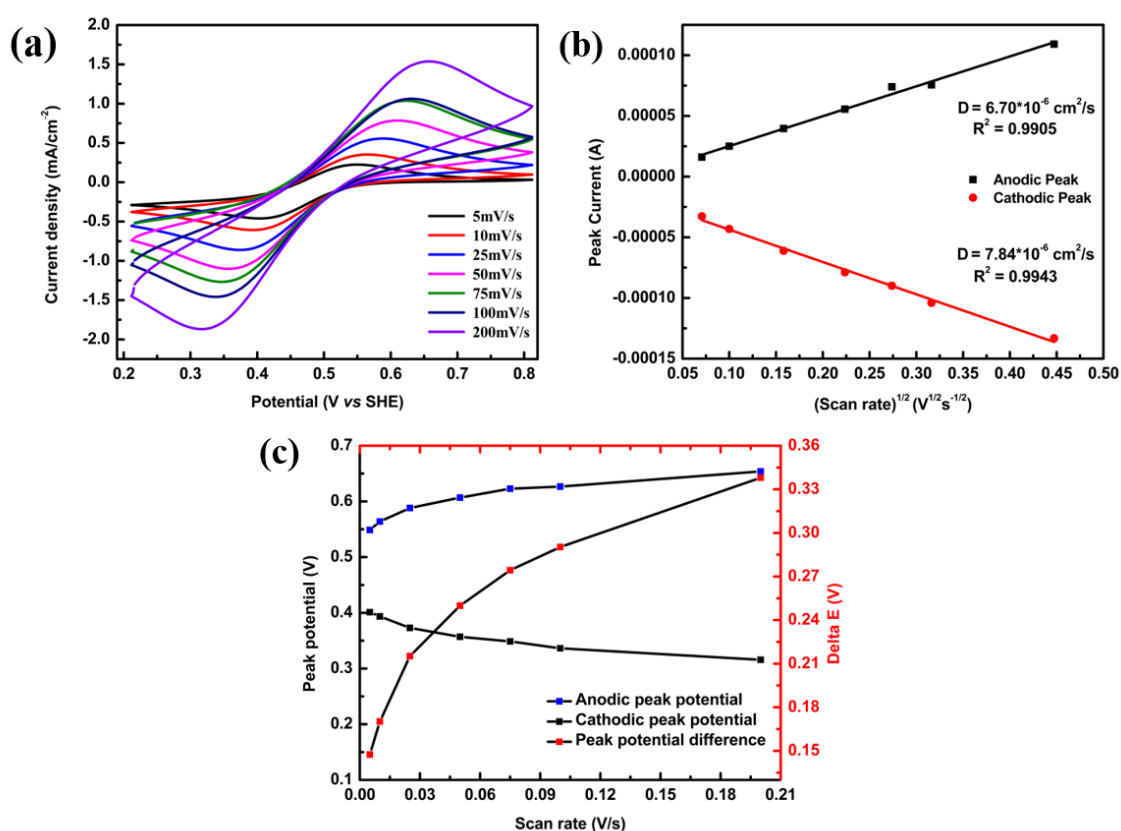

Figure 17: *(a) Cyclic voltammogram of 10 mM ferricyanide in 1M KOH at different scan rate, (b) Plot of peak current vs. square root of scan rate, (c) Plot of anodic and cathodic peak potential vs. scan rate.*

4.3 Electrochemical analysis: Rotating disk electrode (RDE)

4.3.1 Alloxazine ester redox reaction

In order to know the standard electrochemical rate constants of each redox species, rotating disk electrode experiments were carried out and analyzed using the Koutecky-Levich equation. Liner sweep voltammogram of alloxazine ester was recorded at 100mV s^{-1} at different rotation rates between 100 to 1000 rpm on platinum working electrode (Figure 18a). The current plateau of electrochemical was observed at -0.85 V *vs.* SHE, but is not well defined due to the possible absorption of redox species (alloxazine ester) on electrode surface during the experiments. By increasing the rotation rate of the electrode, we observed that current was increasing because current

is related to the rate of mass transport. Therefore, when we have increased the rotation rate, the current was increasing.

The diffusion constant of alloxazine ester was calculated by plotting the limiting current as a function of square root of the rotation rate between -0.6 to -0.9 V *vs. SHE*. It exhibited a straight line, as described by the Levich equation and gave a diffusion coefficient of 1.32×10^{-6} $cm^2 s^{-1}$ (Figure 18b), indicating the fast diffusion of alloxazine molecule. Whereas, the rate constant estimated from Koutecky-Levich analysis for alloxazine ester was found to be 4.79×10^{-4} cm s^{-1}. The rate constant of alloxazine ester suggests a faster-redox reaction kinetic as compared to the one obtained for ACA (1.2×10^{-5} $cm.s^{-1}$), in the same conditions. From Figure 18c, the plot of ln(ik) vs overpotential, we were select some region in the tangent using different overpotential and plotted the Koutecky-Levich plot is linearly with the square root of the scan rate as shown in Figure 18d.

Figure 18: Rotating-disk experiments performed for 10 mM alloxazine ester in 1M KOH solution. (a) LSVs as function of rotation rate (b) Levich plot obtained from figure a, (c) plot of the logarithm of the kinetically limited current against overpotential, (d) Koutecky-Levich plot as a function of overpotential.

4.3.2 KMnO₄ redox reaction

Liner sweep voltammogram of KMnO$_4$ were recorded at 100mV s^{-1} and various rotation speeds. From Figure 19a, the plateaus of electrochemical reduction of permanganate at 0.4V and oxidation of manganate at 0.75V are well defined due to the diffusion-controlled reactions as suggested by the theory of Levich, with the appearance of a sigmoidal shaped-LSV in theses experimental conditions.

The diffusion coefficient of KMnO$_4$ was calculated by plotting the limiting current as a function of square root of the rotation rate. It exhibited straight line following by the Levich equation $1.69*10^{-5}$ cm^2 s^{-1}, indicating the fast diffusion of KMnO$_4$. Whereas, the rate constant estimated from Koutecky-Levich analysis for KMnO$_4$ was found to be $7.47*10^{-4}$ cm s^{-1}, suggesting a fast-redox reaction. There is no report in the literature regarding the diffusion coefficient of KMnO$_4$ in 1M KOH.

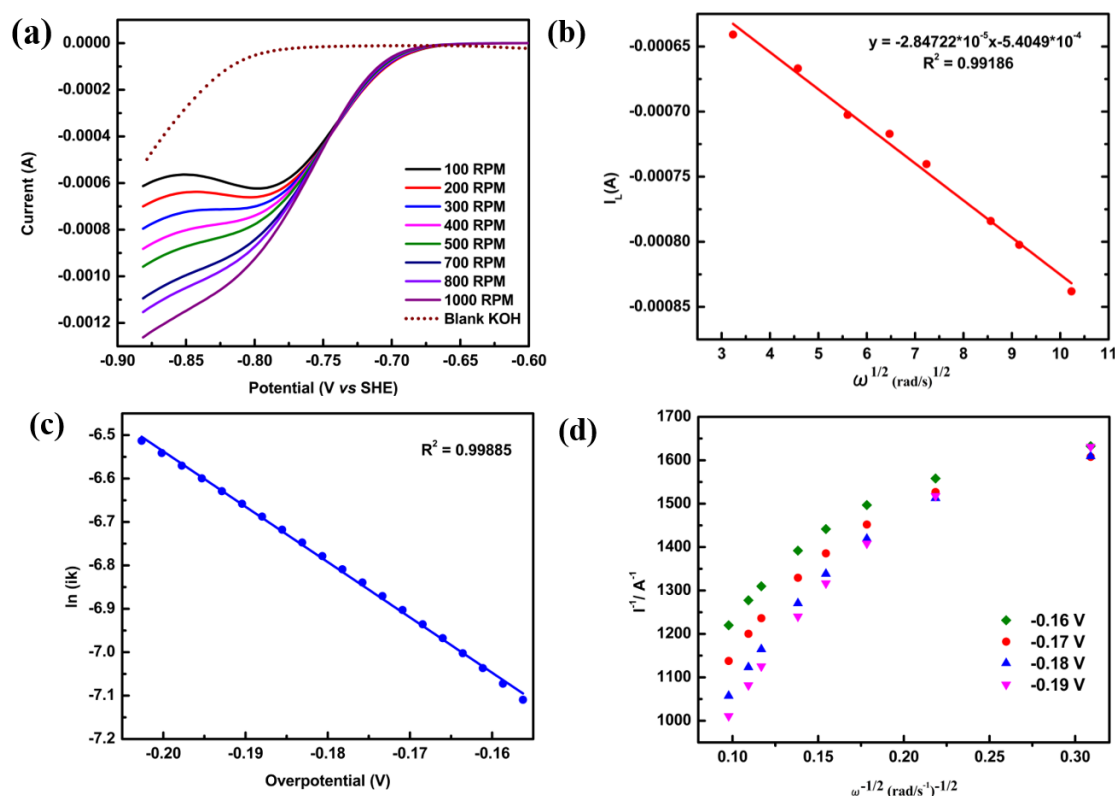***Figure 19:*** *Rotating-disk experiments performed for 10 mM in 1M KOH solution. (a) LSVs as function of rotation rate. (b) Levich plot obtained from figure a, (c) plot of the logarithm of the kinetically limited current against overpotential, (d) Koutecky-Levich plot as a function of overpotential.*

4.3.3 Ferrocyanide redox reaction

Liner sweep voltammogram of ferrocyanide were recorded at 100mV s^{-1} at different rotation speeds. From Figure 20a, the plateau current of electrochemical oxidation of ferrocyanide was observed at 0.7 V *vs.* SHE and well defined due to the diffusion-controlled reactions.

The diffusion constant of ferrocyanide was calculated by plotting the limiting current as a function of square root of the rotation rate. It exhibited straight line following by the Levich equation $1.89*10^{-5}$ cm^2 s^{-1}, indicating the fast diffusion of ferrocyanide. Whereas, the rate constant estimated from Koutecky-Levich analysis for ferrocyanide were $3.30*10^{-1}$ cm s^{-1} respectively further suggesting a fast-redox reaction. The value obtained was similar with literature for ferrocyanide in 1M KOH is $1.68*10^{-1}$cm s^{-1}.[43] In compare to permanganate the ferrocyanide showing a fast redox reaction due to higher rate constant.
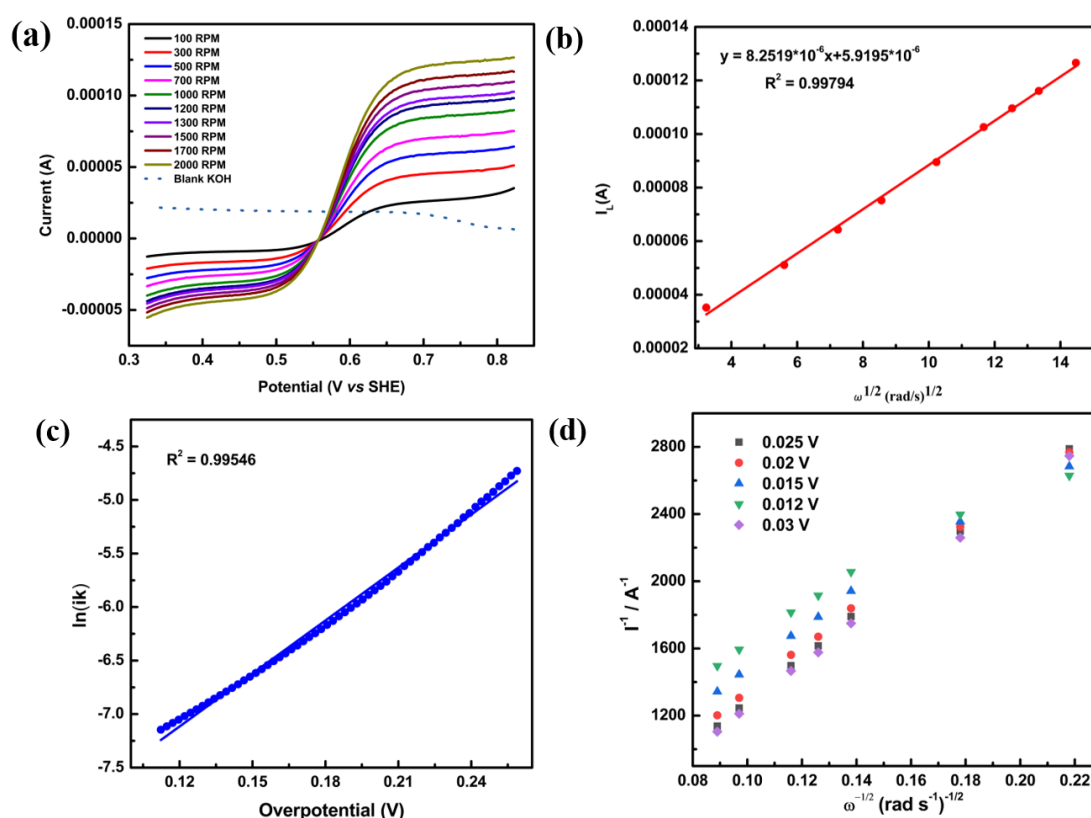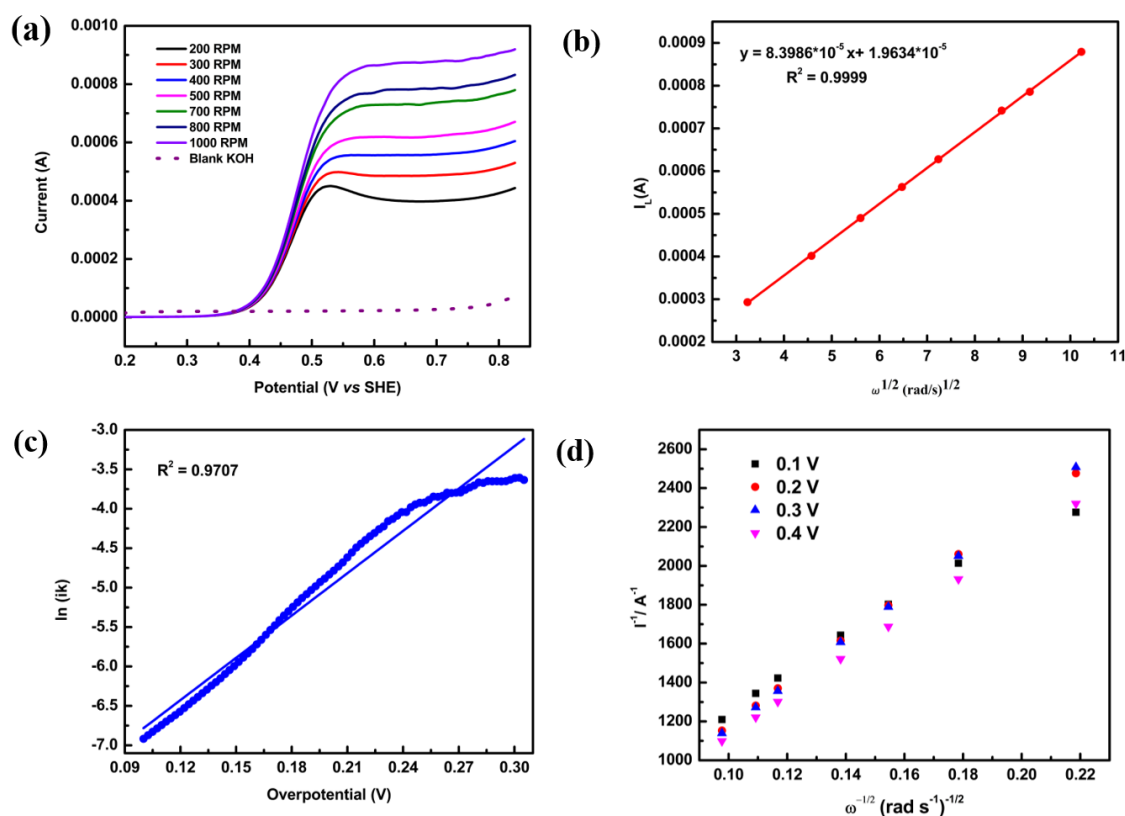

Figure 20: *Rotating-disk experiments performed for 10mM ferrocyanide in 1M KOH solution. (a) LSVs as function of rotation rate (b) Levich plot obtained from figure a, (c) plot of the logarithm of the kinetically limited current against overpotential, (d) Koutecky-Levich plot as a function of overpotential.*

We performed the electrochemical characterization like cyclic voltammetry and rotating disk electrode to know the diffusion coefficient and rate constant of electrolyte such as alloxazine ester, ferrocyanide, $KMnO_4$. The diffusion constant is showing the fast electron transfer kinetics for the alloxazine ester, ferricyanide, $KMnO_4$ and rate constant is showing the faster diffusion of the redox species. For the alloxazine ester is showing the higher rate constant compare to reported alloxazine carboxylic acid by Aziz group. To know the charge/discharge rate and capacity of flow battery we performed the flow cell experiments in higher and low concentration as discussed below.

4.4 Flow cell cycling

Flow cell experiments were performed at different concentrations using alloxazine ester at the negative side and two posolyte ferrocyanide/ferricyanide and KMnO$_4$/K$_2$MnO$_4$ at the positive side.

4.4.1 10mM alloxazine ester *vs.* 50mM ferrocyanide/ferricyanide alkaline RFB

The battery was assembled using 10mM alloxazine ester at the negative side and 50mM ferrocyanide + 50mM ferricyanide at the positive side. Flow cell cycling results are depicted in Figure 21 using the two electrode setup. The battery was charged up to 1.4 V at 100% state-of-charge (SOC) and discharged until 0.9 V. The open-circuit voltage of 1.4V is higher than the aqueous RFB (acidic conditions) because in alkaline we increase the overpotential of OER and HER. In comparison, the theoretical cell voltage of the vanadium redox flow battery is lower and equal to 1.26 V.
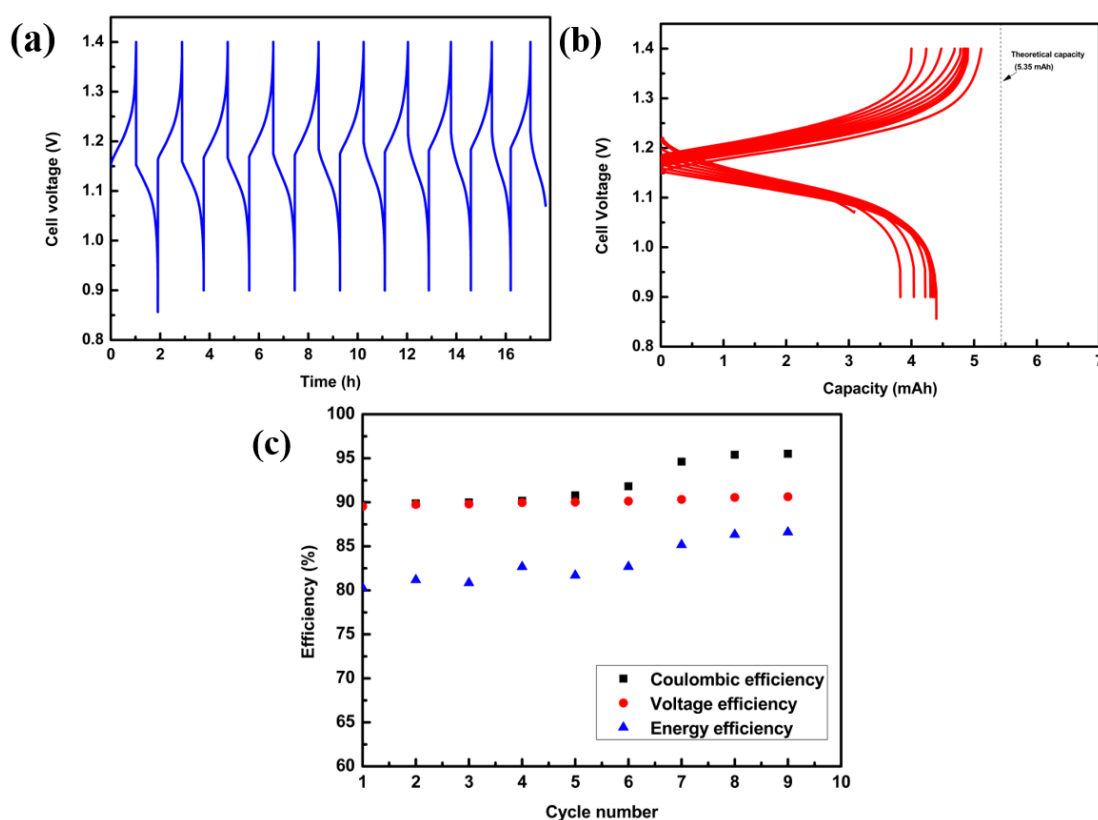

Figure 21: Flow cell cycling: (a)10 cycle of continuous charge and discharge using 10 mL of 10 mM alloxazine ester in 1M KOH as negolyte and 50mM ferrocyanide + 50mM

From Figure 21a, we observe that charge and discharging time are similar over a long period of 16 h. The apparent charging time (total theoretical charge divide by current) of 1.034 h is very close to the theoretical charging time of 1.07 h. However, we did not reach the full volumetric theoretical capacity of the battery (535 mAh L^{-1}), as mentioned in Figure 20b. We achieved only the 450 mAh L^{-1} because of the mass transport limitations and side reactions (OER). After increasing the number of cycle, there is a significant capacity loss because of probable electrolyte degradation (OER) or self-discharge. From Figure 20c, the energy and voltage efficiencies are reasonable (82% and 90%) for such a small concentration of electrolyte. In the high concentration of electrolytes, Aziz group showed an coulombic efficiency of 99.7 %.[29]

4.4.2 10mM Alloxazine ester *vs.* 50mM KMnO$_4$/K$_2$MnO$_4$ alkaline RFB

The battery was assembled using 10mM alloxazine ester and 50mM KMnO$_4$ + 50mM K$_2$MnO$_4$ at the negative and positive sides, respectively. From Figure 22a, we observed that the battery is charged at 1.4 V and discharged at 1 V. Here, we discharged the battery up to 1 V because the standard potential of KMnO$_4$ is around 50 mV higher than ferrocyanide redox couple. We observed that no significant time loss was demonstrated over a long experiment time since the apparent charging time (1.1 h) is equal to the theoretical one. However, we did not reach the full volumetric theoretical capacity of the battery (535 mAh L^{-1}), as mentioned in Figure 22b. We achieved only the 450 mAh L^{-1} volumetric capacity because of the mass transport limitations and side reactions (OER). Oxidation potential of water in alkaline condition is around 0.6 V *vs.* SHE. From Figure 22c, the coulombic efficiency is about 90%, mainly due to electrolyte precipitation on the carbon felt and pipes. Average energy and voltage efficiencies were found to be equal to 81% and 90%.

Figure 22: *Flow cell cycling: (a)10 cycles of continuous charge and discharge using 10 mL of 10 mM alloxazine ester in 1 M KOH as negolyte and 50 mM KMnO$_4$ + 50 mM K$_2$MnO$_4$ in 1 M KOH as posolyte. 5 mA current was applied for charging and discharging of the battery (b) Cell voltage (V) vs. capacity (mAh). (c) Efficiency (%) vs cycle number. Electrolyte flow rate was 21 mL min^{-1}.*

4.4.3 50mM Alloxazine ester *vs.* 50mM KMnO$_4$/K$_2$MnO$_4$ alkaline RFB

The battery was assembled using 50 mM alloxazine ester and 50 mM KMnO$_4$ + 50 mM K$_2$MnO$_4$ at the negative and positive sides, respectively. From Figure 23, we observed that the battery is charged at 1.6 V and discharged at 0.8V. No significant time loss was demonstrated over a long-time experiment since the apparent charging time 1.2 h is equal to the theoretical one. However, we did not reach the full theoretical capacity of the battery 2.68 Ah L^{-1} because of the mass transport limitations and side reactions and we achieved only 1.83 Ah L^{-1}. Here the coulombic efficiency is about 97%, mainly due to platting electrolyte precipitation on the carbon felt and pipes, as seen on Figure 24. MnO$_2$ plating was occurring on the positive side electrode after the cell cycling, as observed by SEM. Average energy and voltage efficiencies of 79% and 77% per cycle were observed .
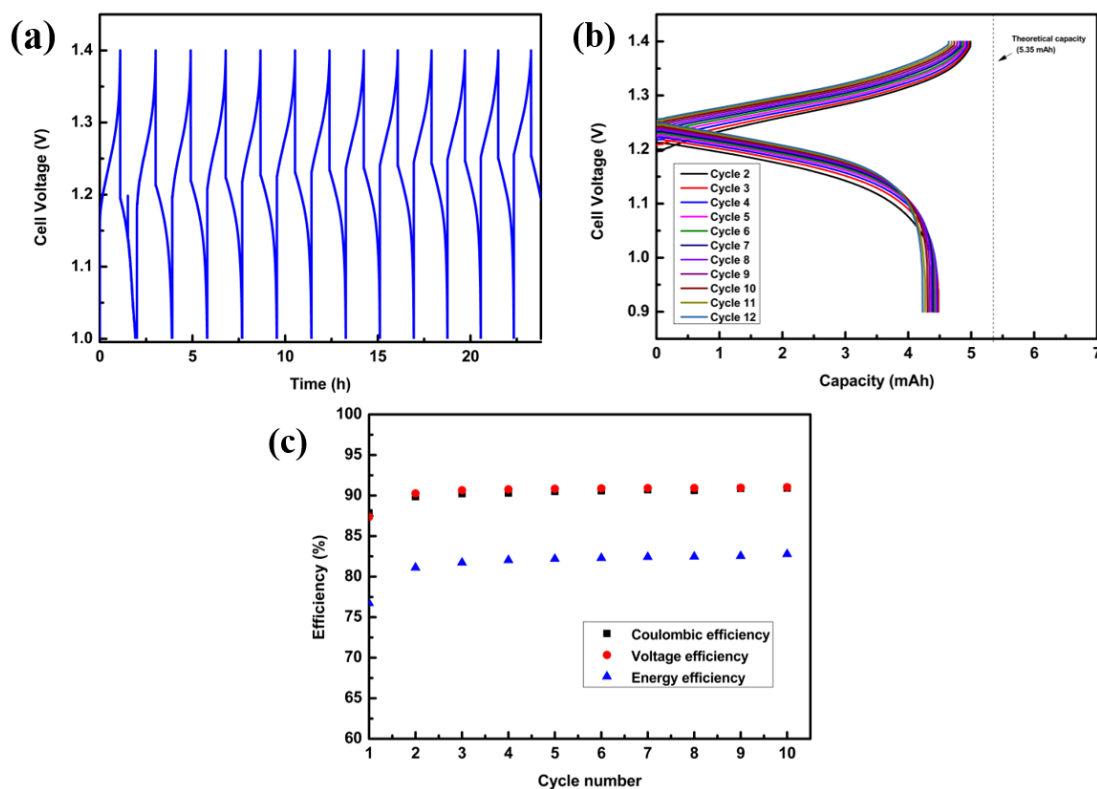
Figure 23: Flow cell cycling: (a)10 cycle of continuous charge and discharge using 10mL of 50 mM alloxazine ester in 1 M KOH as negolyte and 50 mM $KMnO_4$ + 50 mM K_2MnO_4 in 1M KOH as posolyte. 20 mA current was applied for charging and discharging of the battery (b) Cell voltage (V) vs. capacity (mAh). (c) Efficiency (%) vs cycle number. Electrolye flow rate was 21 mL min^{-1}.

To see the battery performance in higher concentration, we were performed the flow cell experiment using the different cationic exchange using Nafion117, Nafion 112, CMVN, CMTN. These membranes are made of different polymers and different thickness. For Nafion 117 membrane, It was prepared through incorporation of perfluoro vinyl ether groups on a polytetrafluoroethylene (PTFE, or Teflon) polymer, with edges of former terminating on sulfonate groups with the thickness of 183 µm and CMTN is cationic exchange membrane which is use for electrodialysis with the thickness of 100 µm. In addition, the mass transport limitations of electrolyte was significantly higher from 50 to 100 mM of electrolyte, to prevent this issue we were changed the battery cell configuration as shown in Figure100 to higher surface area

of electrode (from 2 to 8cm^2) and higher diameter of pipes using three electrode setup to control the charging and discharging potential better on both side of the battery.

Figure 24: *SEM images of the electrode after the cell cycling in different resolution, (a,b) 50mM alloxazine ester in 1M KOH, (c,d) 50mM KMnO$_4$ + 50mM K$_2$MnO$_4$ in 1M KOH.*

4.4.4 100mM Alloxazine ester *vs.* 100mM KMnO$_4$/K$_2$MnO$_4$ alkaline RFB

The battery was performed with Nafion 117 membrane using the 100mM alloxazine ester and 100mM KMnO$_4$ + 100mM K$_2$MnO$_4$ at the negative and positive sides. We observed that no capacity loss up to 30 cycles but the coulombic efficiency was low and equal to 84 %. MnO$_2$ plating was occurring on the positive side electrode and as well as in the pipes after the cell cycling, as confirmed on SEM image of the electrode (Figure 25). Average voltage and energy efficiency are 97 and 81% respectively, are good for the small concentration. However, the full volumetric theoretical capacity of the battery is 5.3 Ah L^{-1} and we achieved 4.8 Ah L^{-1} due to the MnO$_2$ plating on both electrodes and membranes. Figure 25e shows the MnO$_2$ plating on the Nafion 117

membrne after the cell cycling and Figure 26 shows the MnO₂ plating on the electrode surface after the cell cycling as confirmed by the SEM.
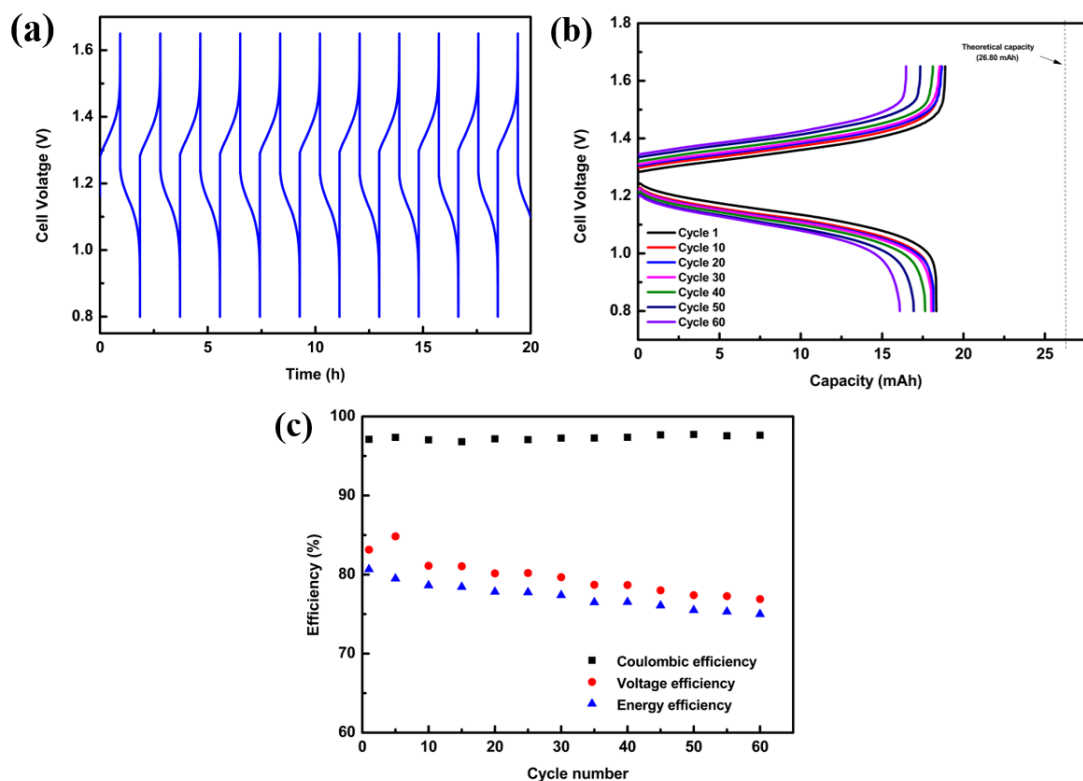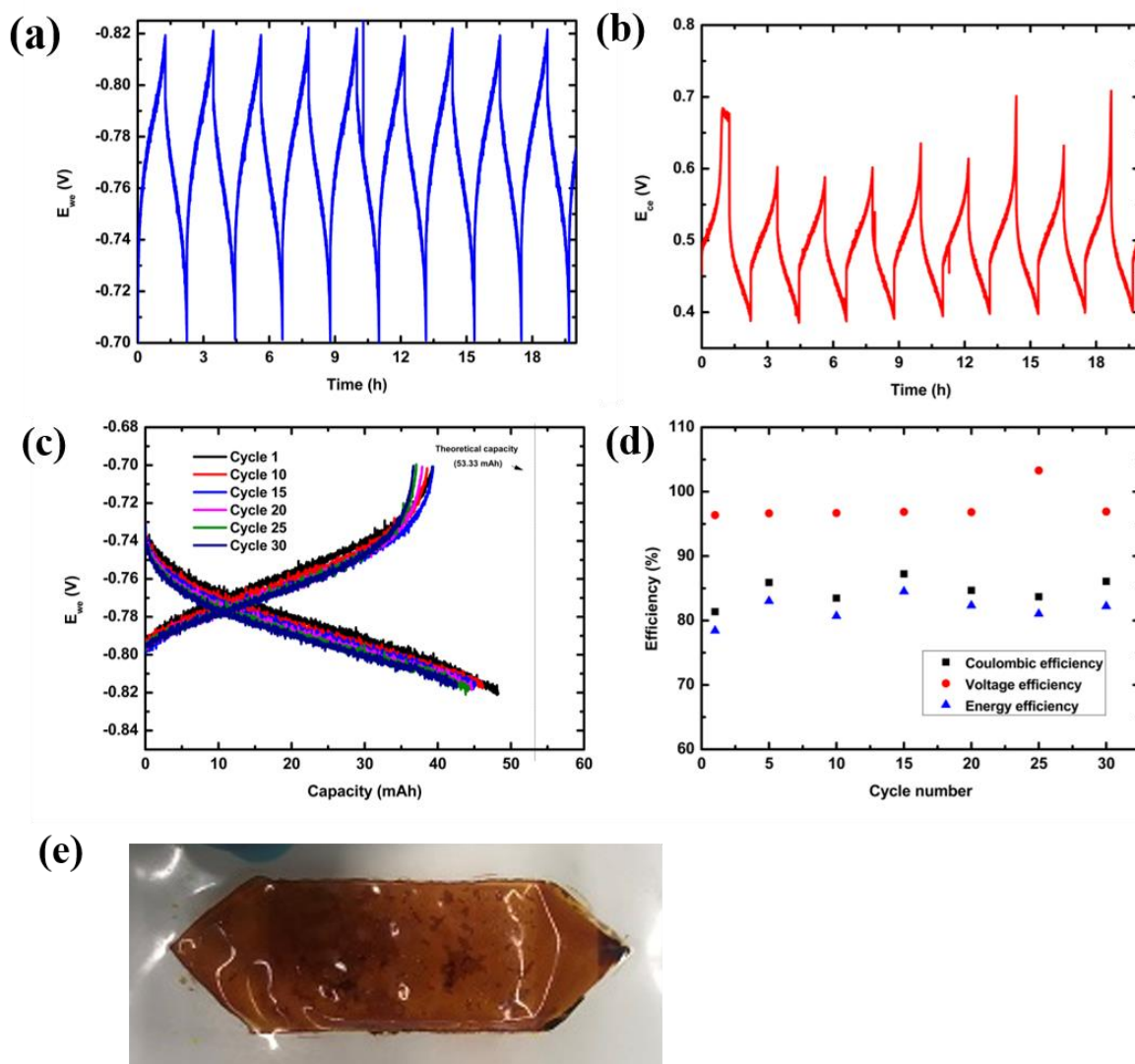

Figure 25: *Flow cell cycling: (a)30 cycle of continuous charge and discharge using 10mL of 100mM alloxazine ester in 1M KOH as negolyte and 30mL 100mM KMnO₄ + 100mM K₂MnO₄ in 1M KOH as posolyte. 150mAcurrent was applied for charging and discharging of the battery, b) Eco vs. time (c) Cell voltage(V) vs. capacity (mAh). (d) Efficiency (%) vs cycle number, (e) Picture of the Nafion 117 membrene after the cell cycling. Electrolyte flow was 25mL min⁻¹.*
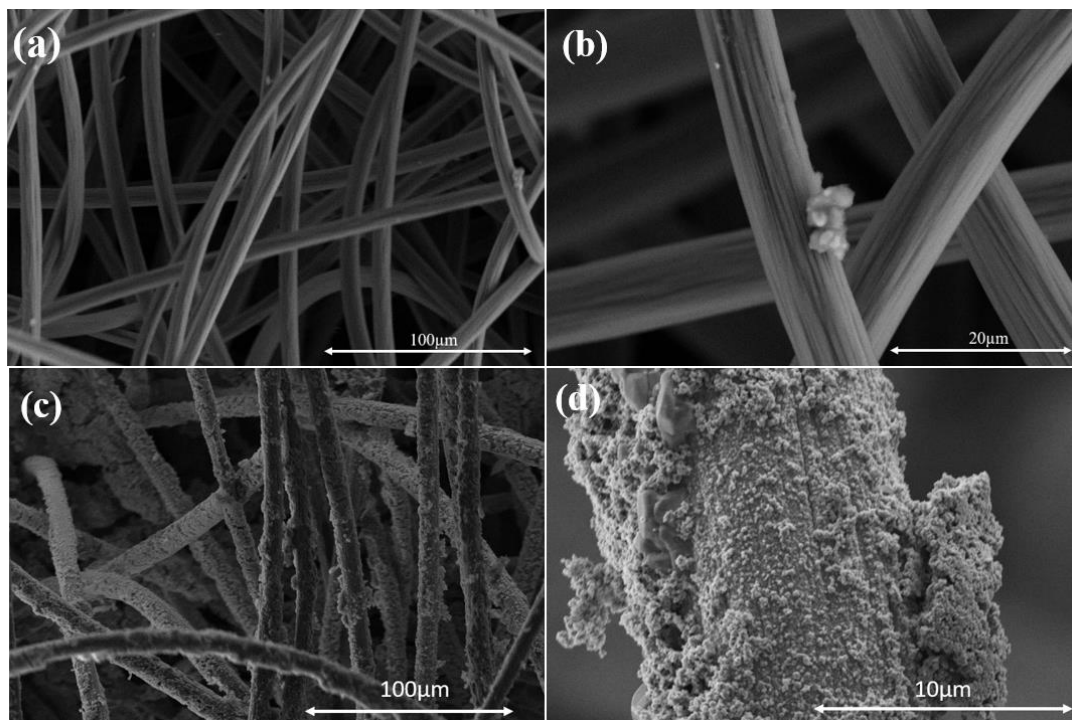
Figure 26: *SEM images of the electrode after the cell cycling in different resolution, (a,b) 100mM alloxazine ester in 1M KOH, (c,d) 100mM $KMnO_4$ + 50mM K_2MnO_4 in 1M KOH.*

In the initial experiment, the battery was performed in small concentration using small cell setup (Figure 9) to know the performances. At low concentration, manganate and ferrocyanide demonstrate the same performance in the terms of energy and voltage efficiencies. Operating the RFB at higher concentrations (100 mM alloxazine ester and 100 mM K_2MnO_4 & 100 mM $KMnO_4$), we observed MnO_2 plating onto the electrodes surface and membrane as well as in the pipes (Figure 26). Other cationic exchange membranes such as Nafion 112, CMVN and CMTN, were tested at the same concentration. Unfortunately, flow cell performances were not better than the one reported above, and severe platting of manganate was observed, which was further confirmed by SEM analysis. Therefore, ferro/ferricyanide redox couple was selected as posolyte in higher concentration to avoid the precipitation.

4.4.5 0.38M Alloxazine ester *vs.* 0.4M ferrocyanide/0.04ferricyanide alkaline RFB

The battery was assembled in higher concentration using 0.38M alloxazine ester and 0.4M ferrocyanide + 0.04 mM ferricyanide in 1M KOH at the negative and positive sides as shown in Figure 27. In this battery, 5mm gold coated titanium current collector was used to present titanium corrosion in alkaline condition (formation of TiO_2). Flow battery was charged and discharged at 150mA. However, the volumetric capacity of the battery is 20.36 Ah L^{-1} and we achieved the 17.41 Ah L^{-1}.
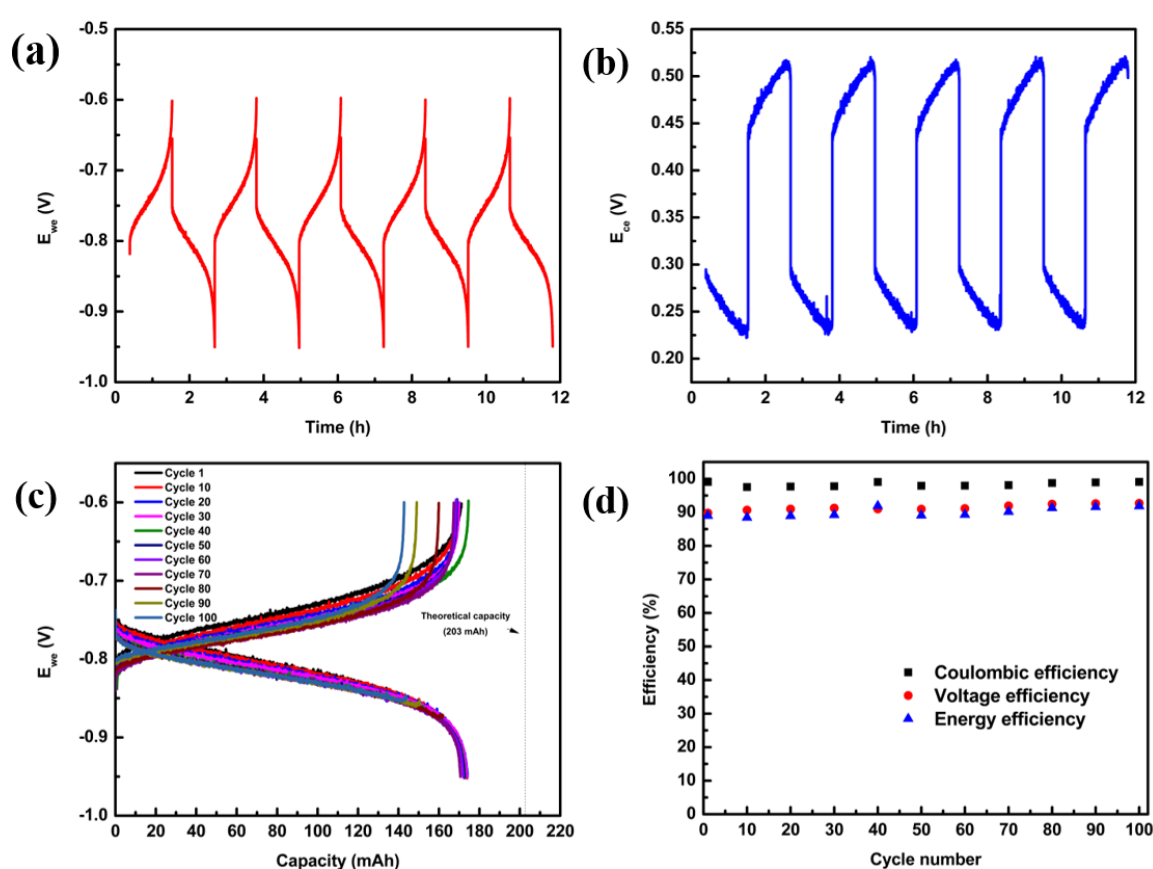
Figure 27: *Flow cell cycling: (a)100 cycle of continuous charge and discharge using 10ml of 0.38M alloxazine ester in 1M KOH as negolyte and 30ml 0.4M ferrocyanide + 0.04mM ferricyanide in 1M KOH as posolyte.150mA current was applied for charging and discharging of the battery, b) Eco vs. time (c) Cell voltage(V) vs. capacity (mAh). (d) Efficiency (%) vs cycle number. Electrolyte flow was 25mL min^{-1}.*

We observed no capacity loss up to 100 cycles with 98.34 % of coulombic efficieny per cycle. Average energy and voltage efficiencies were found to be equal to 91.41% and 90.07% as shown in Figures 27d. From SEM images (Figure 27), no plating on the electrode and membrane were observed.
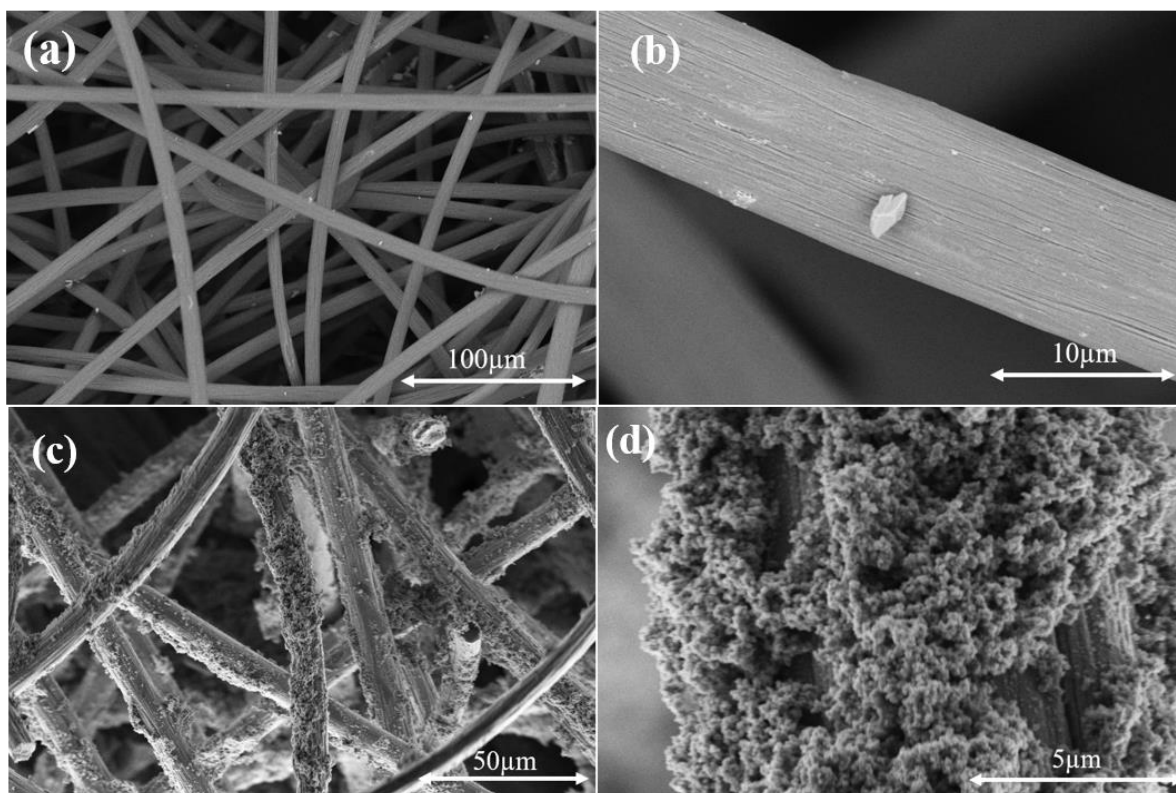

Figure 28: SEM images of the electrode after the cell cycling in different resolution, (a,b) 100mM alloxazine ester in 1M KOH, (c,d) 100mM KMnO$_4$ + 50mM K$_2$MnO$_4$ in 1M KOH.

Conclusion and Perspectives

This work presented the development of the alkaline redox flow battery based on organic based-aqueous electrolytes. The solubility of the electrolytes was characterized by UV-vis spectroscopy and the electrochemical properties of the electrolytes was 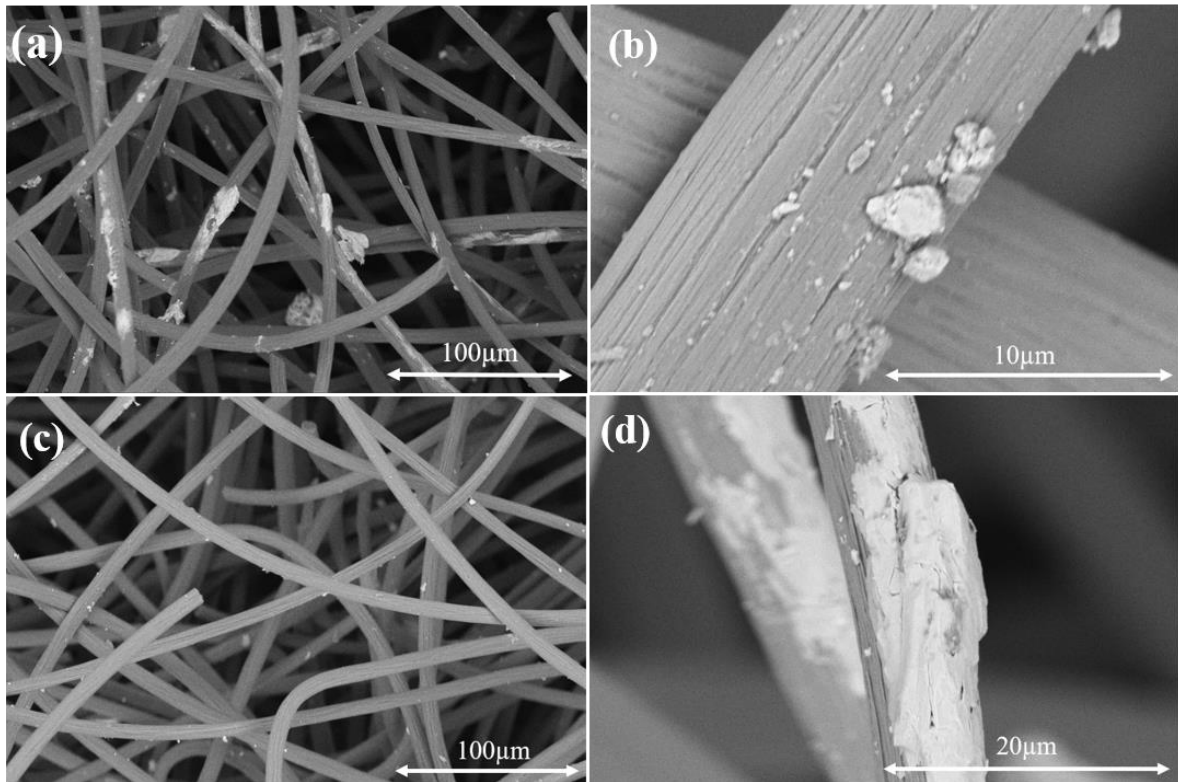characterized by cyclic voltammetry (CV), rotating disk electrode (RDE). We performed the battery using 100mM alloxazine ester and 100mM K_2MnO_4 & 100mM $KMnO_4$ in 1M KOH and we observed that the electrolyte was precipitated and MnO_2 was platted in the pipes as well as on the electrode surface, which was further confirmed by SEM analysis. Then, we performed the flow cell experiments with ferro/ferricyanide to prevent the precipitation issue. In higher concentration we performed the battery using 0.38M alloxazine ester at negative side and 0.4M ferrocyanide &0.04M ferricyanide to demonstrate a high-performance flow battery. The coulombic efficiency exceeded 98.34 % over 100 stable charge/discharge cycles, while voltage and energy efficiency are 91 and 90%. Alloxazine ester is a promising material for the negative side of alkaline redox flow battery.

From further perspectives of this work, to prevent the issue of degradation of alloxazine ester because alloxazine ester is hydrolyzed in the KOH medium to give back the carboxylic acid group. This was observed and conformed by 2D NMR. However, Alloxazine sulfonic acid will be investigated for the alkaline redox flow battery due to slightly higher redox potential than the alloxazine ester.

References

1. Chu, S. & Majumdar, A. Opportunities and challenges for a sustainable energy future. *Nature* **488**, 294–303 (2012).

2. Larcher, D. & Tarascon, J.-M. Towards greener and more sustainable batteries for electrical energy storage. *Nature Chem* **7**, 19–29 (2015).

3. Yang, Z. *et al.* Electrochemical Energy Storage for Green Grid. *Chem. Rev.* **111**, 3577–3613 (2011).

4. Dunn, B., Kamath, H. & Tarascon, J.-M. Electrical Energy Storage for the Grid: A Battery of Choices. *Science* **334**, 928–935 (2011).

5. Dennison, C. R. *et al.* Redox Flow Batteries, Hydrogen and Distributed Storage. *chimia (aarau)* **69**, 753–758 (2015).

6. Hadjipaschalis, I., Poullikkas, A. & Efthimiou, V. Overview of current and future energy storage technologies for electric power applications. *Renewable and Sustainable Energy Reviews* **13**, 1513–1522 (2009).

7. Nitta, N., Wu, F., Lee, J. T. & Yushin, G. Li-ion battery materials: present and future. *Materials Today* **18**, 252–264 (2015).

8. Ponce de León, C., Frías-Ferrer, A., González-García, J., Szánto, D. A. & Walsh, F. C. Redox flow cells for energy conversion. *Journal of Power Sources* **160**, 716–732 (2006).

9. Alotto, P., Guarnieri, M. & Moro, F. Redox flow batteries for the storage of renewable energy: A review. *Renewable and Sustainable Energy Reviews* **29**, 325–335 (2014).

10. Thaller L. H.US Patent N 3,996,064 : Electrically rechargeable redox flow cell, 1976.

11. Posner A. Fuel, 1955, 34, 330–338.

12. Noack, J., Roznyatovskaya, N., Herr, T. & Fischer, P. The Chemistry of Redox-Flow Batteries. *Angew. Chem. Int. Ed.* **54**, 9776–9809 (2015).

13. Weber, A. Z. *et al.* Redox flow batteries: a review. *J Appl Electrochem* **41**, 1137–1164 (2011).

14. Sum, E., Rychcik, M. & Skyllas-kazacos, M. Investigation of the V(V)/V(IV) system for use in the positive half-cell of a redox battery. *Journal of Power Sources* **16**, 85–95 (1985).

15. Rychcik, M. & Skyllas-Kazacos, M. Characteristics of a new all-vanadium redox flow battery. *Journal of Power Sources* **22**, 59–67 (1988).

16. Fang, B. A study of the Ce(III)/Ce(IV) redox couple for redox flow battery application. *Electrochimica Acta* **47**, 3971–3976 (2002).

17. Soloveichik, G. L. Flow Batteries: Current Status and Trends. *Chem. Rev.* **115**, 11533–11558 (2015).

18. Skyllas-Kazacos, M., Cao, L., Kazacos, M., Kausar, N. & Mousa, A. Vanadium Electrolyte Studies for the Vanadium Redox Battery-A Review. *ChemSusChem* **9**, 1521–1543 (2016).

19. Saraidaridis, J. D. & Monroe, C. W. Nonaqueous vanadium disproportionation flow batteries with porous separators cycle stably and tolerate high current density. *Journal of Power Sources* **412**, 384–390 (2019).

20. Singh, V., Kim, S., Kang, J. & Byon, H. R. Aqueous organic redox flow batteries. *Nano Res.* **12**, 1988–2001 (2019).

21. Roznyatovskaya, N., Noack, J., Pinkwart, K. & Tübke, J. Aspects of electron transfer processes in vanadium redox-flow batteries. *Current Opinion in Electrochemistry* **19**, 42–48 (2020).

22. Janoschka, T. *et al.* An aqueous, polymer-based redox-flow battery using non-corrosive, safe, and low-cost materials. *Nature* **527**, 78–81 (2015).

23. Gentil, S., Reynard, D. & Girault, H. H. Aqueous organic and redox-mediated redox flow batteries: a review. *Current Opinion in Electrochemistry* **21**, 7–13 (2020).

24. Ding, Y. & Yu, G. Molecular Engineering Enables Better Organic Flow Batteries. *Chem* **3**, 917–919 (2017).

25. Hu, B., DeBruler, C., Rhodes, Z. & Liu, T. L. Long-Cycling Aqueous Organic Redox Flow Battery (AORFB) toward Sustainable and Safe Energy Storage. *J. Am. Chem. Soc.* **139**, 1207–1214 (2017).

26. Park, M., Ryu, J., Wang, W. & Cho, J. Material design and engineering of next-generation flow-battery technologies. *Nat Rev Mater* **2**, 16080 (2017).

27. Liu, T., Wei, X., Nie, Z., Sprenkle, V. & Wang, W. A Total Organic Aqueous Redox Flow Battery Employing a Low Cost and Sustainable Methyl Viologen Anolyte and 4-HO-TEMPO Catholyte. *Adv. Energy Mater.* **6**, 1501449 (2016).

28. Huskinson, B. *et al.* A metal-free organic–inorganic aqueous flow battery. *Nature* **505**, 195–198 (2014).

29.   Lin, K. *et al.* A redox-flow battery with an alloxazine-based organic electrolyte. *Nat Energy* **1**, 16102 (2016).

30.   Lin, K. *et al.* Alkaline quinone flow battery. *Science* **349**, 1529–1532 (2015).

31.   Orita, A., Verde, M. G., Sakai, M. & Meng, Y. S. A biomimetic redox flow battery based on flavin mononucleotide. *Nat Commun* **7**, 13230 (2016).

32.   Wang, C. *et al.* High-Performance Alkaline Organic Redox Flow Batteries Based on 2-Hydroxy-3-carboxy-1,4-naphthoquinone. *ACS Energy Lett.* **3**, 2404–2409 (2018).

33.   Yang, Z. *et al.* Alkaline Benzoquinone Aqueous Flow Battery for Large-Scale Storage of Electrical Energy. *Adv. Energy Mater.* **8**, 1702056 (2018).

34.   Colli, A. N., Peljo, P. & Girault, H. H. High energy density MnO_4^-/MnO_4^{2-} redox couple for alkaline redox flow batteries. *Chem. Commun.* **52**, 14039–14042 (2016).

35.   Girault, H. H. *Electrochimie physique et analytique*. (2012).

36.   Bard, A. J. & Faulkner, L. R. *Electrochemical methods: fundamentals and applications*. (Wiley, 2001).

37.   Khan, M. S., Asif, A., Khawaldeh, S. & Tekin, A. Dopamine detection using mercaptopropionic acid and cysteamine for electrodes surface modification. *Journal of Electrical Bioimpedance* **9**, 3–9 (2018).

38.   Denuault, G., Sosna, M. & Williams, K.-J. Classical Experiments. in *Handbook of Electrochemistry* 431–469 (Elsevier, 2007). doi:10.1016/B978-044451958-0.50024-0.

39.   *https://pineresearch.com/shop/kb/theory/hydrodynamicelectrochemistry/ rotating-electrode-theory/.*

40.   Chen, R. Toward High-Voltage, Energy-Dense, and Durable Aqueous Organic Redox Flow Batteries: Role of the Supporting Electrolytes. *ChemElectroChem* **6**, 603–612 (2019).

41.   Lee, W., Kwon, B. W. & Kwon, Y. Effect of Carboxylic Acid-Doped Carbon Nanotube Catalyst on the Performance of Aqueous Organic Redox Flow Battery Using the Modified Alloxazine and Ferrocyanide Redox Couple. *ACS Appl. Mater. Interfaces* **10**, 36882–36891 (2018).

42.   Araújo, M. P., Soares, O. S. G. P., Fernandes, A. J. S., Pereira, M. F. R. & Freire, C. Tuning the surface chemistry of graphene flakes: new strategies for selective oxidation. *RSC Adv.* **7**, 14290–14301 (2017).

43.   Luo, J. *et al.* Unraveling pH dependent cycling stability of ferricyanide/ferrocyanide in redox flow batteries. *Nano Energy* **42**, 215–221 (2017).